

Photometric Identification of the Low-Mass Population of Orion OB1b I: The σ Ori Cluster

W. H. Sherry, F. M. Walter

Department of Physics & Astronomy, SUNY Stony Brook, Stony Brook, NY 11794-3800

and

S. J. Wolk²

Center for Astrophysics, 60 Garden Street, Cambridge, MA 02138

ABSTRACT

We report an optical photometric survey of 0.89 deg^2 of the Orion OB1b association centered on σ Ori. This region includes most of the σ Ori cluster, the highest density region within Orion OB1b. We have developed a statistical procedure to identify the young, low-mass, pre-main sequence population of the association. We estimate that the cluster has ~ 160 members in the mass range ($0.2 \leq M \leq 1.0 M_{\odot}$). The cluster has a radius of $\sim 3\text{-}5 \text{ pc}$ and an estimated age of $2.5 \pm 0.3 \text{ Myrs}$. We estimate that the total mass of the cluster is $225 \pm 30 M_{\odot}$. This mass is similar to the estimated mass of the $\sim 5 \times 10^5$ year old cluster NGC 2024. NGC 2024 and σ Ori appear to be a well matched pair of clusters, except for the $\sim 2 \text{ Myr}$ difference in their ages.

Subject headings: open clusters and associations: individual(σ Ori) — stars: formation — stars: imaging — stars: low-mass — stars: pre-main-sequence

1. Introduction

The Orion OB1 association is one of the most intensively studied local star forming regions. Several stages of star formation are observed in Orion OB1 spanning ages from less than 10^6 years up to $\sim 10^7$ years. Orion is notable as the largest nearby site of very recent, perhaps ongoing star formation. Much of this activity is hidden within the main molecular clouds of the Orion Complex, the Orion A and Orion B clouds (Genzel & Stutzki 1989). There are several deeply embedded clusters in the Orion B cloud (L1630 Lada et al. 1991) aside from the well known optically visible OB association.

1.1. The subgroups of Orion OB1

Blaauw (1964) divided the optically visible association into four groups labeled a-d in order of decreasing estimated age. The groups were identified based upon their degree of concentration, their association with interstellar matter, age, and spatial positions. The spatial boundaries of the groups are somewhat arbitrary in part because the photometric overlap between different groups makes it difficult to unambiguously assign individual O and B stars to a particular group (see figure 5 from Blaauw 1964). Also, the large size and low spatial density of association members confuse efforts to determine membership from converging proper motion vectors (Brown, de Geus, & de Zeeuw 1994). The proper motions are very small because Orion lies in the anti-direction of the solar reflex motion.

The nearest and oldest of the sub-associations, Orion OB1a, is roughly 10^7 years old and ~ 330 pc from the Sun (Brown et al. in press). Orion OB1b contains the belt stars and the stars around them, including σ Ori. Orion OB1b lies about 440 pc from the Sun and has an age of 2-5 Myrs (Brown et al. in press). Orion OB1c contains the stars around the sword region. Orion OB1d is the Orion Nebula Cluster (ONC). The ONC lies at a distance of ~ 450 pc and is less than 1 Myr old. Much of the work on Orion OB1 has concentrated on the ONC (e. g. Hillenbrand (1997) in the optical: Garmire et al. (2000); Flaccomio et al. (2003); Feigelson et al. (2003) in X-rays: Carpenter et al. (2001) in the NIR: Stassun et al. (1999); Herbst et al. (2002); Rebull (2001) for photometric variability: Scally et al. (1999); Simon, Close, & Beck (1999) for binaries). See O’Dell (2001) for a recent review.

As a region of active star formation, the ONC provides a look at the final stages of accretion. Orion OB1b, including the σ Ori region, is a fossil star forming region which presents the end products of star formation.

1.2. Clustered Star Formation in Orion

While the ONC is the best known example of clustered star formation in Orion, it is only one of nearly a score of concentrations of very young stars in the Orion OB1 and λ Ori associations. Many of these clusters are deeply embedded within the giant molecular clouds (GMCs) of the star forming region. In addition to the partially embedded ONC, Lada et al. (1991) catalog four embedded clusters within the Orion A clouds and three within the Orion B cloud. These embedded clusters all have radii of roughly 1 pc. This is roughly the same size as the high density cores in GMCs (Lada & Lada 2003). The number of members in these clusters ranges from 43 (L1641N) to >300 (NGC 2024). Carpenter (2000) used 2MASS observations of the Orion A and Orion B clouds to estimate that more than 50% of

all the stars in these clouds are located in clusters.

Gomez & Lada (1998) report three clusters in the λ Ori OB association with radii of $\sim 30'$ (3.5 pc). Roughly 80% of the pre-main sequence (PMS) stars in the λ Ori region belong to one of these three clusters. South of Orion's belt ($\delta < -1.5$) Gomez & Lada (1998) identify seven clusters of low-mass PMS stars among the strong $H\alpha$ sources of the Kiso $H\alpha$ survey (Wiramihardja et al. 1989; Kogure et al. 1989; Wiramihardja, 1991, 1993). Five of these clusters correspond to known clusters of O and B stars: NGC 1977, the ONC, OMC-2, the upper sword, and the lower sword. Two consist solely of low-mass stars.

Lada & Lada (2003) compiled a list of all published embedded clusters within two kpc of the sun. They found that there are several times too many young embedded clusters compared to the number of bound open clusters. They concluded that fewer than 10% of young embedded clusters remain as recognizable entities for more $\sim 10^7$ years after their natal molecular gas is dispersed.

1.3. The σ Ori Cluster

Walter et al. (1998) reported the identification of a concentration of low-mass PMS stars around the O9.5V star σ Ori. Walter et al. (1998) spectroscopically identified 104 PMS stars within $30'$ of σ Ori. Photometry of 0.15 deg^2 containing 45 spectroscopically confirmed PMS stars suggested another 65 likely PMS stars with $V < 19$. With 110 PMS stars in the 0.15 deg^2 area, Walter et al. (1998) concluded that the spatial density of PMS stars was at least 700 deg^{-2} in the region around σ Ori. The spatial density of PMS stars in the spectroscopic survey decreased with distance from σ Ori, indicating that the low-mass PMS population near σ Ori formed part of a cluster with a radius of $\sim 0.5^\circ$.

The σ Ori cluster has since proven to be a rich hunting ground for sub-stellar objects ranging from brown dwarfs (Béjar et al. 1999, 2001; Barrado y Navascués et al. 2003) down to free-floating “cluster planets”. One candidate member has a mass as low as 3 Jupiter masses (Zapatero Osorio et al. 2000, 2002b; Martín & Zapatero Osorio 2003), although Burgasser et al. (2004) suggest that it is a foreground brown dwarf.

Sizes, luminosities, and ages depend upon the assumed distance to the σ Ori cluster. Most papers on the brown dwarf population of the σ Ori cluster have used the Hipparcos distance for σ Ori. Throughout this paper we use the 440 pc distance to Orion OB1b (Brown et al. in press) as the distance to the cluster. We prefer this value to the 350 pc Hipparcos distance to σ Ori (Perryman et al. 1997) because the uncertainties of the Hipparcos measurements in Orion are large and the distance to Orion OB1b is averaged over many stars

(deZeeuw et al. 1999; Brown et al. in press).

1.4. Searching for New Low-Mass PMS Stars

Several methods have been used to identify low-mass PMS stars in Orion and other star forming regions (Walter et al. 2000). $H\alpha$ emission is an efficient means of finding classical T Tauri stars (cTTs). Large scale surveys such as the KISO $H\alpha$ survey (Wiramihardja et al. 1989; Kogure et al. 1989; Wiramihardja, 1991, 1993) have identified many candidate low-mass PMS stars in Orion. A drawback of low resolution $H\alpha$ surveys is that they cannot distinguish between foreground dMe stars and low-mass PMS stars. Also, $H\alpha$ surveys are biased towards finding cTTs which have strong $H\alpha$ emission. Many, if not most of the low-mass members of the σ Ori cluster must be weak T Tauri stars (wTTs) since few of the members have strong $H\alpha$ emission. This is typical of regions where the natal gas has dispersed (Briceño et al. 2001).

Young low-mass stars are magnetically active, which makes them bright X-ray sources. X-ray surveys of star forming regions can detect both the wTTs and cTTs populations. For large survey regions, the ROSAT all sky survey (RASS) may be used to search for low-mass PMS stars (i. e. Sterzik et al. 1995; 2004). The RASS has a limiting flux of $\sim 10^{-14}$ erg cm $^{-2}$ s $^{-1}$. Assuming a typical X-ray to V band flux ratio of 10^{-3} , only PMS stars brighter than $V \sim 15$ could be detected by the RASS (Walter et al. 2000). Also, the RASS sample is strongly contaminated by many young, X-ray active foreground stars which may be mistaken for PMS stars (Briceño et al. 1997).

High to medium resolution spectroscopic observations unambiguously identify young low-mass PMS stars through the detection of the 6707 Å line of Li I which indicates youth (Walter et al. 2000). Spectroscopic observations also distinguish between cTTs and wTTs and yield radial velocities. The primary disadvantage of using spectroscopy to find new low-mass PMS stars is that high or medium resolution spectroscopy of numerous faint stars over many square degrees requires significant amounts of time on large telescopes.

Broad band optical surveys with one meter class telescopes can detect the low-mass PMS stars in young OB associations with reasonable exposure times (Wolk 1996; Briceño et al. 2001, 2002; Sherry 2003). With broad band photometry, the challenge has always been to separate the PMS association members from main-sequence field stars. Variability measurements are an extremely effective technique for identifying young, low-mass PMS stars (Briceño et al. 2001, 2002). However, this method is potentially biased against PMS stars with only low amplitude photometric variations.

Wolk (1996) reported optical (UBVR_CI_C) photometry of X-ray-selected PMS stars near σ Ori. He found that the X-ray-selected PMS stars occupied a distinct locus on the color-magnitude diagram (CMD). Only about half of the stars in this locus were X-ray-selected PMS stars. Spectroscopic observations of 26 non-X-ray detected stars in this PMS locus showed that about 70% were PMS stars. This suggested that the low-mass PMS population in Orion OB1b could be efficiently identified by using single epoch photometry to select the stars which lie in the PMS locus. Single epoch photometry alone cannot definitively identify any individual star as a PMS star, but it can be used to determine the size and spatial distribution of the low-mass PMS population of the association.

1.5. This work

We have completed a BVRI survey of 0.89 deg² around σ Ori. Our data permit us to measure several properties of the σ Ori cluster, including the radius, the total mass, and the age of the cluster. The mass and radius of the cluster determine the escape velocity of the cluster. A small escape velocity would indicate that the cluster is not bound. The total mass and radius of the cluster also provide a context which allows us to look at the σ Ori cluster as part of a hierarchy of star forming regions of various sizes and masses. A reliable age for the cluster will place the cluster and its member stars on an evolutionary sequence with other young clusters such as NGC 2024 and the ONC. Armed with an understanding of the cluster’s mass, radius, and age, we can identify similar clusters at different evolutionary stages, or explore how the richness of clusters influences the evolution of protoplanetary disks.

2. Observations and Data Reduction

In this paper we analyze data from observations made with the 0.9m and 1.5m telescopes at the Cerro Tololo Inter-American Observatory (CTIO) between 1996 and 2002 as part of a B, V, R_C, and I_C survey of the belt of Orion (Orion OB1b). Information about these runs is summarized in Table 1. The positions of our 21 survey fields are shown in Figure 1.

The data from the four 0.9m fields adjacent to σ Ori were observed and reduced by Wolk (1996). These fields were observed only in the V, R_C, and I_C bands. Four fields were observed on the CTIO 1.5m telescope with the Site2K_6 2048×2048 CCD on 1998 December 3. The plate scale of the 1.5m images is 0.43 arcsec/pixel for a field of view of 14.7′×14.7′. The color-balance filter (used to make the spectral energy distribution of the dome flat lights

resemble the twilight sky) was inadvertently left in place for the entire night. This made the limiting magnitude ~ 2 magnitudes brighter for the four fields which were observed that night. Otherwise the photometry was unaffected (see Sherry 2003 for a detailed description of the photometry). The remaining fields were observed on the CTIO 0.9m telescope with the Tek2K_3 2048 \times 2048 CCD between 1998 December 7 and December 11. These observations have a plate scale of 0.4 arcsec/pixel and a field of view of 13.6' \times 13.6'. Twilight flats were taken each night and used as the flat field images for each filter. Observations of standard star fields (Landolt 1992) were made several times per night.

For our 1998 observations we used exposure times of 300 seconds in the B, V, R_C, and I_C bands. With these exposure times we had several saturated stars on almost every image, so we also took short, typically 20 seconds, exposures in each band. This allowed us to avoid saturating most of the stars in our fields.

We observed 6 control fields with the same instrument between 2002 January 4 and January 9. Our control fields cover an area of 0.27 deg². The control fields were chosen to have a Galactic latitude of -18.4 and a Galactic longitude of 190.1 which is similar to the Galactic latitude and longitude of Orion OB1b at $-17, 205$. The observing procedure and data processing were identical to the 1998 run.

2.1. Aperture Photometry

We used IRAF¹ to process and reduce these data. We used the QUADPROC routine to trim, bias subtract, and flat field each image. For each of our science fields we used the DAOFIND routine to select stars in the R band image. We removed saturated stars, bad pixels, and cosmic rays from our source list. We then ran the DAOPHOT aperture photometry routine with our R band source list to measure the instrumental magnitudes of all the stars in each band. We used an aperture with a radius of 2.4" (6 pixels) for our 1998 science fields. For our 2002 fields we used a smaller aperture with a radius of 1.2" (3 pixels).

¹IRAF is the Image Reduction and Analysis Facility. It is distributed by the National Optical Astronomy Observatories, which is operated by the Association of Universities for Research in Astronomy, Inc., under contract with the National Science Foundation.

2.1.1. *Photometric Calibration*

All the nights of our 1998 and 2002 runs were photometric. We observed several standard star fields (Landolt 1992) at the beginning and end of each night. We also observed one or two selected Landolt fields several times each night. In 1998 we used an aperture of $7.1''$ (18 pixels) to measure instrumental magnitudes of Landolt standards. For the 2002 run we used an aperture of $6.7''$ (17 pixels). We used the IRAF PHOTCAL routines to solve for the zero point, extinction and color terms of the standard star solution. The residuals from the standard star solutions were 1% to 2% each night.

2.1.2. *Aperture Corrections*

We used an aperture correction to place our photometry on the same system as our standard fields. The PSF of the CTIO 0.9m telescope varies noticeably with position on the CCD because the focal plane of the telescope is curved. This is insignificant for large apertures, but can be a few percent for an aperture of $2.4''$ or $1.2''$.

The spatial dependence of the aperture correction varies with the focus, so every image is slightly different. We accounted for the spatial dependence of the aperture correction in each image by fitting the aperture corrections for stars with photometric errors less than 0.02 magnitudes by a quadratic function of the distance from the center of the image and linear functions of the X and Y pixel positions. This allowed us to determine the aperture correction for each star with an uncertainty of about 0.01 magnitudes. For a detailed look at the spatial dependence of the aperture corrections for the 0.9m telescope see Sherry (2003).

2.1.3. *Completeness*

For each of our three observing runs we estimated the completeness limits of our observations by counting the number of stars as a function of magnitude. We used the magnitude at which the number of stars per magnitude bin ended its rapid rise and began to decrease as the completeness limit for that field. The 1996 run on the CTIO 0.9m telescope had a V band completeness limit of 18.5 (Wolk 1996). Our 1998 observations on the CTIO 1.5m telescope had a V band completeness limit of 18. Our 1998 observations on the CTIO 0.9m telescope had a V band completeness limit of 20. The spatial distribution of our fields makes our completeness limit about $V=18$ within $\sim 0.3^\circ$ of σ Ori and 20 for regions more than $\sim 0.3^\circ$ from σ Ori.

2.1.4. Astrometry

We determined positions in pixel coordinates with the Gaussian centroiding algorithm of the PHOT routine. We used D. Mink’s *imwcs* program (Mink 1997)² to determine the astrometric solution for each image by fitting the pixel coordinates of our targets to the known positions of USNO-A2.0 astrometric standards located in each field. For a typical 300s exposure we matched ~ 150 stars with an average residual of $\sim 0.3''$. We then calculated the mean position of each star by averaging the positions found in each of the V, R_C , and I_C images. This allowed us to reduce the uncertainty in the relative position of each star to about $0.1''$. This is consistent with the centering errors returned by the DAOPHOT Gaussian centroiding algorithm. The accuracy of the absolute positions is limited by the USNO-A2.0 catalog which has systematic errors of $< 0.25''$ (Monet et al. 1998).

3. Analysis

Figure 2 shows the V versus $V-I_C$ CMDs for the 0.89 deg^2 around σ Ori and the 0.27 deg^2 of our control fields. The left panel of Figure 2 shows a noticeable increase in the density of stars on the CMD near the position of the 2.5 Myr isochrone (Baraffe et al. 1998; Baraffe et al. 2001). This is in sharp contrast to the CMD of our control field (right panel). An extrapolation from the control fields suggest that there should be ~ 45 field stars near the 2.5 Myr isochrone our survey region around σ Ori. In fact there are roughly 250 stars near the 2.5 Myr isochrone. We interpret this significant excess population of stars as the PMS population of the σ Ori cluster.

The non-negligible background of field stars in the PMS locus makes it impossible to securely identify individual PMS stars using only single epoch photometry. Since we cannot securely identify individual PMS stars photometrically, we have to identify the PMS population statistically. Attempts to reliably estimate the number of cluster members from the statistically identified PMS population are complicated by the non-uniform density of field stars along the PMS locus. There is a higher density of field stars in the PMS locus for $V-I_C < 1.5$ and possibly for $V-I_C > 3$. The variation in the field star contamination of the PMS locus necessitates that we estimate both the density of PMS stars and the density of field stars at each point on the color-magnitude diagram.

In Figure 2 we can follow the PMS locus between $V-I_C=1.6$ and $V-I_C=3.2$. Blueward of $V-I_C=1.6$ the PMS locus intersects the field star distribution and is too weak to trace. The

²Documentation and source code are available at <http://tdc-www.harvard.edu/software/wcstools/>

PMS locus becomes less distinct redward of $V-I_C=3.2$ ($V\sim 19$) because redder PMS stars would be fainter than the limiting magnitude of our fields closest to σ Ori. Our observations of the outer reaches of the cluster are deeper, but the density of PMS stars is lower, so we detect field stars but very few PMS stars with $V>19$.

3.1. Statistical Identification of Cluster Members: Cross-Sections through the CMD

We analyzed our data more quantitatively by counting the number of stars as a function of $V-I_C$ color and V magnitude along a series of cross-sections perpendicular to the PMS locus. We found that the distribution of stars along cross-sections through the CMD is well represented by the sum of a Maxwellian-like distribution of field stars and a Gaussian distribution of PMS stars. An example of one of these cross-sections is shown in Figure 3. We interpret the number of stars under the Gaussian component of the fit as the number of PMS stars in that cross-section. We fit the field and PMS distributions jointly. The distribution of field stars is not interesting per se, but it is critical because the number of PMS stars depends upon the extrapolation of the field star distribution through the PMS locus. A poor fit to the field star distribution could contribute a significant error to the estimated number of PMS stars.

For each cross-section we counted the number of stars in bins along the cross-section and fit the number of stars per bin to a function of the form

$$\frac{N_f}{(e^{a(x-\mu_1)} + 1)(e^{b(x-\mu_2)} + 1)} + N_p e^{-0.5((x-\mu_p)/\sigma)^2}.$$

The first term describes the distribution of field stars and the second term is a Gaussian distribution of PMS stars. We use a least-squares fit performed by the IDL program MPFITFUN (Markwardt 2002) to solve for eight parameters, N_f , a , μ_1 , b , μ_2 , N_p , μ_p , and σ . Table 2 provides a brief description of these parameters. Starting values as well as upper and lower limits for each parameter were estimated from trial fits.

The scientifically significant parameters N_p , μ_p and σ , describe the PMS population. The total number of PMS stars along a cross-section is determined by N_p , the normalization of the Gaussian fit to the PMS distribution, and σ determines the width of the Gaussian. The full width at half maximum (FWHM) of the PMS population is $2\sigma\sqrt{2\ln(2)}$. The μ_p parameter is the $V-I_C$ color of the peak of PMS population along a cross-section. Since each cross-section is a predefined line across the CMD, μ_p determines the V magnitude of the peak of the PMS distribution.

The lower panel of Figure 3 shows a cross-section through the CMD of our control field. The fit is good with $\chi_\nu=1.4$. There was no need for a Gaussian component to the fit for our 0.27 deg^2 control field. The upper panel of Figure 3 shows that the same cross-section through the CMD for our fields near σ Ori has an excess of stars at the expected position of the PMS locus.

We can fit cross-sections over limited a range of $V-I_C$. The red limit on our fits is near $V-I_C=2.9$ because that is where the PMS locus approaches the V band completeness limit of our survey. We are able to fit the PMS locus as far as $V-I_C=3.2$, but we are biased towards detecting mainly the brighter PMS stars at those colors. The blue limit is near $V-I_C=1.6$ because the initial mass function produces fewer stars with increasing mass and the PMS locus intersects the giant branch near $V-I_C=1.5$. This makes the signal to noise of the PMS locus very low for $V-I_C < 1.6$. The number of PMS stars in the region near σ Ori is the sum of the area under the Gaussian components of all of the cross-sections.

The membership probability for each star is the ratio of the Gaussian component of the fit to the sum of the field star and Gaussian components of the fit along each cross-section through the CMD. Membership probabilities calculated this way range from 0% far from the PMS locus to >90% near the peak of the PMS distribution in many cross-sections.

3.2. Comparisons with Theoretical Models

Masses and ages for cluster members can be estimated by comparing the observed population to theoretical models. We chose to compare our data with the models of the Lyon group (Baraffe et al. 1998; Baraffe et al. 2001) because these models incorporate realistic, non-grey stellar atmospheres as their outer boundary conditions. This is very important for low-mass stars because the atmospheres of stars with $T_{eff} \leq 4000 \text{ K}$ form molecules such as TiO, VO, and H₂O. These molecules dominate the spectral energy distribution of the star and control the outer boundaries of the interior models because the top of the convection zone lies close to or within the photosphere (Allard et al. 1997). The Lyon models are the most consistent with the empirical masses, luminosities, and colors of low-mass stars in multiple systems such as GG Tau (White et al. 1999; Simon et al. 2000) and YY Gem (Torres & Rebass 2002). The models of the Lyon group are also consistent with the estimated luminosities and effective temperatures of low-mass PMS stars with masses determined from the orbital velocities of their circumstellar disks (Simon et al. 2000).

Our observational data consist of magnitudes and colors for each star. The Lyon group calculates absolute V band magnitudes as well as optical and near IR colors for their models

from their non-grey model atmospheres. Their magnitudes seem to be accurate in the near IR, but are known to have serious problems in the optical, and especially in the V band (Baraffe et al. 2001). We prefer to use an empirical relationship to estimate the bolometric corrections and colors from the effective temperatures of the models. This allows us to compare theoretical models to the observed CMD.

Published lists of effective temperatures and colors for main sequence stars (Kenyon & Hartmann 1995; Leggett et al. 2001, 2002) make it relatively easy to construct an empirical color-temperature relation. Effective temperatures for very young, low-mass PMS stars ($\tau < 10$ Myr) have not been determined directly from observations of angular diameters. They must be estimated by comparison with spectra from either main sequence or giant stars. Luhman (1999) found that the spectra of M type PMS stars in the ~ 3 Myr old cluster IC 348 were best described by spectra that were the average of main sequence and giant stars of the same spectral type. This is significant because dwarfs and giants of spectral type M have effective temperatures that differ by up to a few hundred Kelvin (Herbig 1977; Walter et al. 1994).

Luhman (1999) constructed an intermediate temperature scale for PMS stars by constraining the Lyon group’s models to match the observed luminosities of the four stars of the GG Tau system to a single age while also matching the observed locus of members of IC 348 at a single age. Enforcing coevality on these populations resulted in a temperature scale that is intermediate between dwarfs and giants.

We constructed an approximate color-temperature relation by combining the colors and bolometric corrections of main sequence dwarfs with the temperature scale constructed by Luhman (1999). We used colors and bolometric corrections from Kenyon & Hartmann (1995) for spectral types earlier than M7 and from Leggett et al. (2001, 2002) and Berriman et al. (1992) for later spectral types. Our color-temperature relation is given in table 3.

There are several caveats associated with this color-temperature relation. First, as Luhman (1999) points out, his temperature scale was designed to make tracks from the Lyon group match PMS stars in IC 348 (age ~ 3 Myr) and the GG Tau quadruple system. As low-mass PMS stars evolve towards the main sequence they contract. An ideal color-temperature relation would have to be a function of age (and metallicity). Luhman’s temperature scale may apply only to the Lyon groups tracks because altering the temperature scale could compensate for shortcomings of the model isochrones.

We did not take differences between the colors of dwarfs and giants into account in table 3 because the colors of later M type giants are uncertain. For K stars, the color difference between dwarfs and giants is modest, less than 0.1-0.2 mag in V–I (Amado &

Byrne 1996). Both the NIR and optical colors of low-mass PMS stars seem to be closer to those of dwarfs than to giants (Luhman 1999; Walter et al. 1994). This suggests that any correction to the colors of PMS stars due to surface gravity effects should be only a small fraction of the color difference between late M type dwarfs and giants. However, the V–I colors of late M giants (Perrin et al. 1998) are >0.5 mag. redder than the colors of late M type dwarfs. A correction for later spectral types could be very important, up to few tenths of a magnitude, for $V-I_C > 3.2$, but this is unlikely to be a serious problem for this data set because we follow the PMS locus reliably only to about $V-I_C \sim 3.2$.

We also made no attempt to correct our color-temperature relation for the effect of star spots on the colors of PMS stars. Gullbring et al. (1998) discusses the differences between the colors of wTTs and main sequence stars with spectral types between K7 and M1. They report PMS stars with color anomalies of up to ~ 0.2 mag in $V-I_C$ and 0.7 mag in $V-K$. In figure 1 of Gullbring et al. (1998) the magnitude of these color anomalies varies by a factor of several among different stars. These color anomalies are consistent with models of PMS stars that have spots over very large fractions of their surfaces. This effect is certainly large enough to be important, but there is insufficient data to correct for it over a wide range in temperature. Also, the magnitude of these color anomalies may vary significantly from star to star. For now, it is impossible to account for these color differences.

3.2.1. Contributions to the width of the PMS Locus

For a given age and composition, theoretical isochrones are one dimensional: luminosities and effective temperatures depend on only the star’s mass. This is appropriate for clusters of main sequence stars because all the members of a cluster have the same age and chemical composition. A cluster’s main sequence will have a small observed width due to binaries, the depth of the cluster along the line of sight, and photometric errors. Young low-mass PMS stars are more complex because all stars are variable at ages less than 10^7 years. The character and strength of the photometric variability depends on the star’s magnetic activity, the amount of circumstellar matter, and the accretion rate. Also, in very young regions such as the ONC (~ 1 Myrs) or the σ Ori cluster (~ 3 Myrs), the relative ages of stars may differ significantly because the period over which the stars formed could be as large or larger than the mean age of the population.

Young low-mass stars ($M < 2 M_\odot$) are placed into two classes: the cTTs and the wTTs. Classical T Tauri stars are actively accreting gas from circumstellar disks. Accretion drives rapid, irregular photometric variability with amplitudes up to 3 magnitudes in the V band (Herbst et al. 1994). Some of this variability is due to hot spots heated by accretion onto

the star. Some is due to obscuration of the star by circumstellar matter (Herbst et al. 1994; Dullemond et al. 2003).

Weak T Tauri stars are not actively accreting significant amounts of mass. These young stars have spots which cover a large fraction (up to 40%) of their surface area (Herbst et al. 1994). They vary periodically as they rotate because they are covered by an asymmetric distribution of spots. They are also chromospherically active which leads to occasional flaring. Weak T Tauri stars vary with amplitudes of ~ 0.05 to ~ 0.6 magnitudes in the V band (Herbst et al. 1994). By an age of a few times 10^6 years, most low-mass stars are wTTs.

Even a population dominated by wTTs will occupy a wide band across the CMD. To compare with a theoretical isochrone we must define the center of the PMS locus. This may not correspond perfectly with the luminosities and temperatures predicted by models, but it is a well defined, measurable line on the CMD.

Many of the factors which contribute to the observed width of the PMS locus should be more or less symmetric about the middle of the locus. We expect that a distance spread would (most likely) follow a Gaussian distribution. Photometric errors are presumed to be Gaussian. Rotational modulation should be symmetric about the mean magnitude of the star because over the course of a rotation we see the entire the visible surface of the star. Stars that have large areas covered by spots must have a somewhat different bolometric correction than would be appropriate for a star with the effective temperature of the immaculate photosphere (which dominates the photosphere in the V band). Optical magnitudes predicted from theoretical isochrones using the bolometric correction of the immaculate photosphere will be systematically brighter than the observed center of the PMS locus because spots redistribute flux out of the optical and into the IR. This will make the PMS population match to a slightly older isochrone.

Variations due to variable accretion or obscuration by circumstellar matter are probably not symmetric about the mean brightness of any individual star. Flaring would make stars brighter, but we expect few stars to have been flaring during the half hour duration of a typical observation. Unresolved binaries are always brighter than single stars. We expect that only $\sim 30\%$ of the stars will have unresolved binary companions and that a typical binary companion will be significantly fainter than the primary. Simulations of the σ Ori populations (Sherry 2003; Sherry, Walter, & Wolk in preparation) suggest that binaries shift the center of the PMS locus to a position only slightly brighter and redder than the center of the PMS locus for single stars.

3.2.2. Age of the Cluster

From Figure 2, it is clear that the 2.5 Myr isochrone is a reasonable fit to the PMS locus. We estimate the age of the cluster more quantitatively by finding the isochrone with the minimum χ_ν^2 . Since we measured cross-sections with bins which were much wider than the spacing between cross-sections, we calculated χ^2 using only every sixteenth cross-section, yielding five independent cross-sections to use when calculating χ_ν^2 .

In Figure 4 we plot reduced χ_ν^2 as a function of age. There is a broad minimum in χ_ν^2 for ages between 2.4 Myrs and 2.6 Myrs. A model with an age of 2.44 Myrs has the smallest χ_ν^2 , but all models with ages between about 2.4 Myrs and 2.6 Myrs have $\chi_\nu^2 \approx 1.7$.

We used the distribution of χ_ν^2 as a function of age to estimate the uncertainty in the cluster’s age (Lampton, Margon, & Bowyer 1976). The dashed lines in Figure 4 mark the expected reduced χ_ν^2 of the 68% and the 90% confidence intervals.

Our best estimate of the age of the σ Ori cluster is 2.5 ± 0.3 Myr (90% confidence). This age is consistent with the ~ 3 Myr age Martín & Zapatero Osorio (2003) found from their distance independent fit to the spectrum of a possible three Jupiter mass member of the σ Ori cluster. An age of ~ 3 Myrs is also consistent with the 2-4 Myr age estimated from the large abundance of Li observed in cluster members (Zapatero Osorio et al. 2002a).

Figure 5 shows the best fit position of the center of the σ Ori PMS locus along with the best-fit isochrone. The short lines mark the $\pm 1\sigma$ position of the center of the PMS locus for each cross-section. It is clear that the isochrone matches the center of the PMS locus quite well. This is not surprising because our color-temperature relation uses the M type temperature-scale which (Luhman 1999) adjusted to make the 3 Myr Lyon group isochrone match the PMS locus of the cluster IC 348.

The quoted uncertainty of ± 0.3 Myrs considers only the random error from the fit to the isochrone. An alternative approach to estimating the random uncertainty in our age estimate would be to examine the width of the PMS locus. The FWHM of the Gaussian fits to our cross-sections corresponds to an uncertainty of ± 1 Myrs. This is a significant overestimate of the uncertainty because the width of the PMS locus is most likely dominated by the photometric variability of the cluster members, not by an age spread (Sherry 2003). We conclude that that the best estimate of the random uncertainty is ± 0.3 Myrs.

The true uncertainty must be larger because there are contributions to the width of the PMS locus, such as spots, which may systematically shift the center of the PMS locus. These systematic errors are difficult to quantify without careful modeling. Uncertainties in the models and the color-temperature relation contribute a systematic error to the absolute

age of the cluster. This is probably the dominant uncertainty in the absolute age, but it is difficult to estimate.

4. Membership and Total Mass of the σ Ori Cluster

The number of PMS stars in a cross-section is determined by integrating the area under the Gaussian component of the fit for that cross-section. We estimate the number of the PMS stars by summing the areas under all of the cross-sections that have high enough signal to noise for us to find a reliable fit through the PMS locus. The cluster does not have a sufficiently rich population of stars with $M \gtrsim 1M_{\odot}$ for us to find a reliable fit to that population. Fainter than our completeness limit of $V=18$ mag, there are also not enough PMS stars to get a good fit through the PMS locus. This limits us to estimating the number of cluster members with $1.59 \leq V-I_C \leq 2.92$. Using the models of the Lyon group and our color-temperature relation (table 3) this color range corresponds to the mass range $0.2 \leq M \leq 1.0M_{\odot}$. In this mass range we count 140 ± 10 stars.

We define the probability, P_{mem} , that any observed star is a cluster member as $P_{mem} = \frac{Fit_{mem}}{Fit_{total}}$, where Fit_{mem} is the amplitude of the Gaussian component of the fit for the cross-section appropriate to the observed color and magnitude of the star. Fit_{total} is defined as the total amplitude of the fit, including both the field and cluster member distributions. Table 4 lists data for all likely cluster members in our survey region in order of decreasing membership probability. The bulk of the probable cluster members listed in Table 4 have $P_{mem} < 70\%$, but we include stars with P_{mem} as low as 10% to provide a complete list of possible cluster members detected by our survey.

4.1. How Does the σ Ori IMF Compare to the Field IMF?

Since our data are complete only in the mass range ($1.0M_{\odot} \geq M \geq 0.2M_{\odot}$), we must assume an initial mass function (IMF) to estimate true central density and total mass of the σ Ori cluster. In all cases we have used the IMF from Kroupa (2002) with $\alpha_3=2.7$. As can be seen in Figure 6, this IMF is consistent with our data. We estimated the mass for individual stars (the last column in Table 4) by first using the observed $V-I_C$ colors and our color-temperature relation (Table 3) to estimate T_{eff} for each star. We then assigned each star the corresponding mass from the 2.5 Myr Lyon group isochrone.

4.2. The Structure of the σ Ori Cluster

Figure 7 shows the spatial distribution of 140 stars that have $P_{mem} > 40\%$. The concentration of cluster members near σ Ori is more easily seen in the radial profile of the cluster (Figure 8). The spatial density of the cluster reaches 0 between $25'$ and $40'$ from σ Ori (3.2 pc and 5 pc).

The projected density in our innermost bin is ~ 1500 stars deg^{-2} within a radius of $3'$, or 25 stars pc^{-2} within a radius of 0.38 pc at a distance of 440 pc. We can place a lower limit on the central density of the cluster by assuming that the stars are uniformly distributed along the ~ 10 pc diameter of the cluster. This (unrealistic) distribution would have a central density of 2.5 stars pc^{-3} in the mass range $0.2 \leq M \leq 1.0 M_{\odot}$. A better estimate of the central density of the cluster requires a model of the spatial distribution of cluster members.

The distribution of stars gives some clues to the dynamical history of the cluster. Given the small number of observed cluster members and the absence of radial velocity or proper motion data for individual cluster members, a simple dynamical model of the cluster suffices to describe the cluster. Open clusters and the ONC have radial profiles which are consistent with King models.

4.2.1. King Model

A simple King model (Binney & Tremaine 1987) is described by three parameters, the central density ρ_0 , the King radius r_0 , and the tidal radius r_t . King models are often described in terms of their concentration, which is defined as $c \equiv \log_{10}(r_t/r_0)$. All King models with the same concentration have the same structure, but differ in scale.

A simple King model assumes equal mass stars in a fully relaxed system. These assumptions are questionable for the σ Ori cluster because it has members which range in mass from $< 0.01 M_{\odot}$ to $\sim 20 M_{\odot}$. Also, a cluster with an age of 3 Myrs may not be relaxed because it has probably existed for only a few crossing times. The cluster has a diameter of 6-10 pc and ~ 400 stars (see section 4.3). If we assume a velocity dispersion of 2 km s^{-1} then the crossing time, t_{cross} , is 3 to 5 Myr, which is longer than the age of the cluster. This underestimates the number of crossing times because, like the ONC (Hillenbrand & Hartmann 1998), the cluster is almost certainly expanding due to the loss of gas after the stars formed.

A system reaches equipartition of energy in a time which is about the same order of

magnitude as the relaxation time,

$$t_{relax} = \frac{0.1N}{\ln N} \times t_{cross}$$

(Binney & Tremaine 1987). For a cluster with roughly 400 stars the relaxation time is $\sim 7 \times t_{cross}$. If the σ Ori cluster had a few crossing times before it lost its gas and began to expand, then the cluster is partially relaxed. To the extent that the cluster is relaxed, stars of different masses will have different velocity dispersions. There are models which account for stars of different masses, but with 140 stars in our sample, very little velocity data, and the large uncertainties in the observed radial profile, there is little justification for fitting a more complex model.

We fit our data with King models that had concentrations ranging from 0.5 to 2.5. We found that our data only weakly constrain the concentration of the King models. This is a result of the large uncertainties on the spatial density of PMS stars in each of our radial bins, especially the bin closest to σ Ori and in the outer regions of the cluster. Deeper observations of the inner 10' of the cluster, needed to improve the measured radial profile, will be reported in a forthcoming paper (Sherry, Walter, & Wolk in preparation).

Models with concentrations between 0.8 and 1.8 fit the cluster's radial profile well. Models which fit our data with statistically reasonable values of χ^2_ν have King radii ranging from 0.4 to 2.0 pc and central densities ranging from 2.5 stars pc^{-3} to 20 stars pc^{-3} ($0.2 \leq M \leq 1.0 M_\odot$). Models with greater concentrations generally fit best with smaller King radii and larger central densities than models with lower concentrations.

The left panel of Figure 8 shows the radial profile of the cluster. The radial profile peaks at the position of σ Ori. The solid curve is our best fit King model. The right panel of Figure 8 shows the spatial density of field stars in the same radial bins used in the radial profile for cluster members. The radial profile of field stars is flat. A two-sided KS test finds that these profiles are different at the 99.9% confidence level.

The King model in Figure 8 has a concentration of 1.1 with a core radius of 1.6 pc, a central density of 3 stars pc^{-3} ($0.2 \leq M \leq 1.0 M_\odot$), and a tidal radius of ~ 20 pc. The tidal radius is not well constrained by our data. At radii greater than 30' or 40' from σ Ori, the density of cluster members is less than the density of our field star contamination, and the error bars for the outer radial bins are too large to constrain the tidal radius. Our data constrain the tidal radius only for very low-concentration models ($c < 0.6$) which have best fitting tidal radii less than 4 pc (30'). Most of these models fit with $\chi^2_\nu > 2$.

To find the true central density, we scale the IMF to match the observed central density of 3 stars pc^{-3} in the mass range $0.2 \leq M \leq 1.0 M_\odot$. This produces a central density of

8 stars pc^{-3} in the mass range $0.08 \leq M \leq 50 M_{\odot}$. The central density must be underestimated since our data do not extend to the center of the cluster because the inner arc-minute of the cluster was excluded to avoid the glare produced by the 3.8 magnitude σ Ori. As a result, the central density of the cluster must be higher than our best fit King models indicate.

4.3. The Total Mass of the Cluster

Our survey identified 140 ± 10 cluster members in the mass range $0.2 \leq M \leq 1.0 M_{\odot}$. It is clear from Figure 1 that our survey did not cover all of the outer regions of the cluster. Our spatial coverage was incomplete on the eastern side of the cluster (near the Orion B cloud) because we excluded several fields ($\sim 0.2 \text{ deg}^2$) where the extinction (at least for field stars) was significantly larger than over most of the cluster. The density of cluster members in the outer regions of the cluster is roughly 100 ± 50 members deg^{-2} . The excluded area should have $\sim 20 \pm 10$ cluster members. This puts the total number of cluster members in the mass range $0.2 \leq M \leq 1.0 M_{\odot}$ at 160 ± 15 .

We assumed that any binaries with separations greater than 1600 AU ($3.6''$) would have been detected as two separate stars. Duquennoy & Mayor (1991) found that 58% of all systems containing G dwarfs are multiple systems. Roughly half of these systems have semi-major axes of less than 1600 AU. Assuming that the binary population of the σ Ori cluster is the same as the field, 30% of observed cluster stars should harbor an unresolved binary companion. Since the IMF is fairly steep, many of these unresolved companions would be below our lower mass limit.

Utilizing the IMF, we estimate that a population with 160 primaries in our mass range $0.2 \leq M \leq 1.0 M_{\odot}$ should consist of 400 stars with $0.072 \leq M \leq 50 M_{\odot}$ and 200 brown dwarfs with $M \geq 0.01 M_{\odot}$. The total predicted mass is $160 M_{\odot}$ in stars and $8 M_{\odot}$ in brown dwarfs. This mass is probably something of an underestimate because the cluster may have an excess number of high mass stars ($M > 3 M_{\odot}$; see below).

4.3.1. Is the Cluster IMF Top-Heavy?

The total mass of a low-mass cluster is strongly dependent on the masses of the few highest mass stars in the cluster. If stars have masses randomly drawn from the IMF, the number of stars in any mass range will vary stochastically. In terms of $\frac{\delta N}{N}$, the largest variations will be among the highest mass stars because there are only a few stars in the highest mass range. In a population of 400 stars randomly drawn from the field IMF, the

expected number of stars with $M \geq 3 M_{\odot}$ is 4 ± 1.5 .

Brown, de Geus, & de Zeeuw (1994) conducted a recent study of the high mass members of the Orion OB1 association. Table 5 lists all 13 stars from Brown, de Geus, & de Zeeuw (1994) within $\sim 30'$ of σ Ori that have spectral types earlier than A0. All 13 of these stars lie within the boundaries of the b subgroup. These are not necessarily all members of the b subgroup, since there is substantial overlap between the a and b subgroups (Lesh 1968; Briceño et al. 2001; Sherry 2003). This is in part due to the arbitrary boundaries of the subgroups (see section 1.1). Figure 9 shows the distribution of stars which Brown, de Geus, & de Zeeuw (1994) selected as members of the Orion OB1a, Orion OB1b, and Orion OB1c subgroups. The distribution of stars starkly illustrates the arbitrary boundaries which have defined the Orion subgroups from the earliest identification of the subgroups (Blaauw 1964) through the massive survey of Warren & Hesser (1977a,b, 1978), and up to the present day. From Figure 9 one can see that several of the B stars considered members of Orion OB1b must be members of Orion OB1a (or possibly Orion OB1c) because the spatial distribution of Orion OB1a surrounds Orion OB1b. We estimate that one to three of the B stars within $30'$ of σ Ori are members of the a or c subgroups. This leaves ten to twelve likely cluster members with $M \geq 3 M_{\odot}$. This is two to three times the number of O and B stars which the field IMF predicts for a population of 400 stars.

We ran several Monte Carlo simulations of the population of the σ Ori cluster to estimate the probability that we would observe one O9 star or about ten stars with $M \geq 3 M_{\odot}$. Each simulated population was constructed by generating stars with masses drawn randomly from the IMF. All simulations assumed that the unresolved binary fraction was 30%. The binary companion's mass was also drawn randomly from the IMF. The simulations continued to generate stars until there were a specified number of primary stars within the chosen mass range (usually $0.2 \leq M \leq 1.0 M_{\odot}$). Each Monte Carlo simulation generated 10,000 simulated populations. The results of these simulations are summarized in Figure 10.

σ Ori is a quadruple system with two stars between $15 M_{\odot}$ and $20 M_{\odot}$. Only about 14% of our simulations with 160 primaries in the mass range $0.2 \leq M \leq 1.0 M_{\odot}$ have a single star in the mass range $15 < M < 25 M_{\odot}$. Slightly more than 85% of our simulated populations do not have any stars with $M \geq 15 M_{\odot}$. This suggests that the number of cluster members is less than would be expected for a population with a $20 M_{\odot}$ star, but the chances of forming such a massive star are not unreasonably small.

Only $\sim 1.4\%$ of our simulation have ten or more stars with masses greater than $3 M_{\odot}$. The fraction of simulations with a given number of high-mass stars rises rapidly as the number of stars with $M \geq 3 M_{\odot}$ falls. A total of 3.5% of our simulations have nine or more stars with $M \geq 3 M_{\odot}$ and 7.6% have eight or more stars with $M \geq 3 M_{\odot}$. The likelihood

of forming 10-13 stars is relatively small. This may indicate that the IMF is slightly top heavy in the cluster, or that we have underestimated the number of high-mass members of Orion OB1a/OB1c which are projected onto the cluster, or that we have underestimated the number of cluster members in the mass range $0.2 \leq M \leq 1.0 M_{\odot}$.

One possibility is that the best fit King model is correct and the σ Ori cluster extends to a larger radius with a low-surface density in the outer regions. The radial profile of the σ Ori cluster falls to the expected level of contamination from field stars (~ 50 stars deg^{-2}) at a radius of $\sim 30'$. We assumed that the tidal radius would be about $30'$ (3-4 pc) as well. The King model from Figure 8 predicts about 80 additional cluster members at distances of more than $30'$ from σ Ori. This would bring the total number of stars in the cluster to about 500.

Another possibility is that the estimated number of low-mass stars ($0.2 \leq M \leq 1.0 M_{\odot}$) and n_3 , the observed number of high-mass stars ($M \geq 3 M_{\odot}$), are both right, but the assumed IMF is not right. Kroupa (2002) lists two values for the slope of the IMF for stars with $M > 1 M_{\odot}$. For the case where unresolved binaries (mostly low-mass companions) are ignored, the Salpeter slope of $\alpha_3 = 2.3 \pm 0.3$ is listed. Sagar & Richtler (1991) showed that when the number of undetected low-mass companions are accounted for, the true slope of the IMF must be steeper than the Salpeter value because the low-mass companions increase the number of low-mass stars. Kroupa (2002) adopts a value of $\alpha_3 = 2.7 \pm 0.3$. This is the value which we used in our simulations. A 1σ decrease to a value of $\alpha_3 = 2.4$ increases the fraction of simulated populations with $n_3 \geq 10$ to 21%. Using the Salpeter value for α_3 we found that nearly 50% of the simulation predict $n_3 \geq 10$. This may indicate that our simulations underestimate the number of undetected binaries. Overall, we conclude that the number of low-mass stars which we observe is not inconsistent with the 13 O and B stars which lie within $30'$ of the center of the cluster.

4.3.2. *The Total Mass of the Cluster*

Panel A of Figure 10 shows the distribution of total masses expected for a population of stars with 160 primaries in the mass range $0.2 \leq M \leq 1.0 M_{\odot}$. The peak of this distribution is at $\sim 165 M_{\odot}$. This value underestimates the mass of the σ Ori cluster because a typical simulation has only half as many high-mass stars as are observed in the cluster. We decided that we could better estimate the total mass of the cluster by separately estimating the mass in stars with $M \geq 3 M_{\odot}$ and in stars with $M < 3 M_{\odot}$. Table 5 lists the estimated masses of likely O and B members of the σ Ori cluster.

The combined mass of the first eleven stars in table 5 is $80 M_{\odot}$. This value is probably accurate only to $\pm 10 M_{\odot}$ because we have no way to definitively distinguish the B stars which are members of the foreground Orion OB1a association from the B stars which are cluster members. We exclude the last two stars in table 5 because they are the most distant from the cluster center and more likely to be foreground to the association.

Panel B of Figure 10 shows the distribution of simulations as a function of the mass in stars with $M < 3 M_{\odot}$. The most likely total mass in stars that have $M < 3 M_{\odot}$ is $144 \pm 28 M_{\odot}$. We estimated the uncertainty by running simulations using inputs that were $\pm 1 \sigma$ from the nominal values of the number of stars in our mass range, the three stellar components of the multipart IMF (Kroupa 2002), and for the boundaries of our mass range. Including stars of all masses, we estimate a total mass of $225 \pm 30 M_{\odot}$ for the σ Ori cluster.

5. Discussion

Photometry is an appealing method for identifying the PMS population of the σ Ori cluster because it requires relatively little observing time and a small telescope. Our photometric selection of likely cluster members is sufficient to deduce the radial profile of the cluster. Determination of other properties of the cluster, such as its expansion age, require kinematic data.

5.1. Is the Cluster Bound?

Given its relatively small mass, it is unlikely that the σ Ori cluster is bound. Radial velocity data (Walter et al. 1998) place an upper limit of 5 km s^{-1} on the velocity dispersion of cluster members. In the absence of a directly measured velocity dispersion, we assume the cluster’s velocity dispersion to be similar to that of the ONC. In the ONC, the velocity dispersion is a function of mass (Hillenbrand & Hartmann 1998), with an average velocity dispersion of $2.34 \pm 0.09 \text{ km s}^{-1}$ (Jones & Walker 1988). Hillenbrand & Hartmann (1998) found a velocity dispersion of 2.81 km s^{-1} for stars between 0.1 and $0.3 M_{\odot}$. The velocity dispersion is lower for the higher mass stars. Van Altena (1988) found a velocity dispersion of $1.49 \pm 0.2 \text{ km s}^{-1}$ for the 50 brightest (hence most massive) members of the ONC. Based upon this we assume that the σ Ori cluster should have a velocity dispersion of $\sim 2 \text{ km s}^{-1}$.

Any bound cluster must have a velocity dispersion which is less than the escape velocity, $v_{esc} = \sqrt{2GM/R}$. Using a total mass of $225 M_{\odot}$ and a radius of 3 pc , $v_{esc} \sim 0.8 \text{ km s}^{-1}$. Even with a larger mass of $300 M_{\odot}$, v_{esc} is still 0.9 km s^{-1} . Unless the cluster has a velocity

dispersion which is much smaller than 2 km s^{-1} , the cluster cannot be gravitationally bound.

5.2. Comparison with the ONC and Other Young Clusters in Orion

The ONC is the most intensively studied part of the Orion OB1 association. Hillenbrand & Hartmann (1998) describe the structure of the ONC in terms of a King model. The ONC has at least 3500 members, a central density of $2 \times 10^4 \text{ stars pc}^{-3}$ and a core radius of $\sim 0.2 \text{ pc}$. The σ Ori cluster has only $\sim 10\%$ of the mass of the ONC.

In terms of its total mass, the σ Ori cluster is similar to the embedded cluster at the heart of NGC 2024 (the Flame Nebula). The NGC 2024 cluster lies within a pocket in the Orion B cloud about $15'$ east of ζ Ori (Barnes et al. 1989; Meyer 1996). The central ionizing source of NGC 2024 may be IR2b, a late O or early B star (Bik et al. 2003). Comerón, Rieke & Rieke (1996) estimated an age of $\sim 2 \text{ Myr}$ for the cluster based upon the frequency of circumstellar disks. Both Liu et al. (2003) and Meyer (1996) found that the cluster has an age of less than 1 Myr based upon a comparison between cluster members and theoretical isochrones on the CMD. The estimated total cluster mass of $\sim 200 M_{\odot}$ (Comerón, Rieke & Rieke 1996) is similar to the $\sim 225 M_{\odot}$ we estimate for the total mass of the σ Ori cluster. The NGC 2024 cluster has an estimated radius of $\sim 10'$ or about 1 pc (Lada et al. 1991). The central density of NGC 2024 exceeds $4000 \text{ stars pc}^{-3}$ (Lada et al. 1991). This is much higher than the central density of the older, more relaxed σ Ori cluster which probably has a central density of $\sim 8 \text{ stars pc}^{-3}$.

The similarity in total mass and the mass of the most massive star (O9V for σ Ori and O8V-B2 for IRS2b [Bik et al. 2003]) make the σ Ori and NGC 2024 clusters an excellent matched pair for examining the evolution of young stars, young clusters, and circumstellar disks between the ages of ~ 0.5 and 2.5 Myr .

5.3. Near-IR Excesses Among Cluster Members

Most of the likely cluster members from our survey were detected by the 2MASS NIR survey. We used the 2MASS data to examine likely cluster members for NIR excesses due to circumstellar disks. Figure 11 shows the J–H vs. H–K color-color diagram of likely members of the σ Ori cluster. The solid line traces the locus of main sequence stars on this color-color diagram. The dashed line marks the upper boundary of the region occupied by reddened stars. Stars with large NIR excesses would lie to the right of the solid line. There are no stars that lie very far from the reddening vector of low-mass stars. The 2MASS data

provide no evidence that any of the cluster members have an optically thick circumstellar disk. However, near-IR observations are not sensitive to the cool disks that may surround the lowest-mass members of the cluster.

Oliveira et al. (2004) conducted a JHK_sL' survey of 24 representative members of the σ Ori cluster plus four members chosen because they are known IRAS sources. They found K_s–L' excesses in 13 of the 24 representative members. Similar results were found by (Jayawardhana et al. 2003) who found that two of their sample of six likely cluster members had K–L' excesses. This suggests that at least 50% of the cluster members retain an optically thick circumstellar disk.

The lack of strong NIR excesses may be in large part because most of the stars in this sample have rather cool temperatures. Stars with effective temperatures below 3000 K have spectral energy distribution that peak in the NIR. Only a fairly luminous disk could contribute a significant fraction of the star's flux in the K band. Alternatively, the members of the σ Ori cluster could have disks which have large inner holes.

6. Conclusions

It is possible to use single epoch optical photometry to statistically identify the low-mass PMS population of nearby, young clusters and associations. This method is complementary to surveys such as that of Briceño et al. (2001) which identify likely PMS stars from their variability. Variability surveys provide a more secure identification of PMS stars, but may be biased to the most variable members of the PMS population. Single epoch photometry can identify the whole PMS population on a statistical basis (at the price of greater contamination from field stars). The size and spatial distribution of the PMS population may be determined through single epoch photometry, although individual stars can be securely identified as PMS stars only through follow up spectroscopy.

In a region such as the σ Ori cluster, the high density of PMS stars makes the number of field stars in the PMS locus relatively small. In associations with a lower density of PMS stars there will be greater contamination of the PMS locus by field stars. For associations with few stars or a very low surface density of low-mass members this method will not work well because the contrast between the PMS population and the field population will be very small.

The σ Ori cluster has an age of 2.5 ± 0.3 Myr. The low-mass members of the cluster have a spatial distribution which is broadly consistent with a King model. The relatively small number of stars in our sample can only weakly constrain the parameters of a King model.

The radius of the cluster is about 30' (3.5 pc). We estimate that the total mass of the σ Ori cluster is $\sim 225 \pm 30 M_{\odot}$. This is very similar to the NGC 2024 cluster, but roughly 10 times less massive than the ONC. With such a small mass, the cluster cannot be gravitationally bound unless it has an unexpectedly small velocity dispersion.

This publication makes use of data products from the Two Micron All Sky Survey, which is a joint project of the University of Massachusetts and the Infrared Processing and Analysis Center/California Institute of Technology, funded by the National Aeronautics and Space Administration and the National Science Foundation.

This research has made use of the USNOFS Image and Catalogue Archive operated by the United States Naval Observatory, Flagstaff Station (<http://www.nofs.navy.mil/data/fchpix/>)

REFERENCES

- Allard, F. Hauschildt, P. H. Alexander, D. R. & Starrfield, S. 1997, ARA&A, 35, 137
- Amado, P. J. & Byrne, P. B. 1996, IrAJ, 23, 177
- Baraffe, I. Charbrier, G. Allard, F. & Hauschildt, P. 1998, A&A, 337, 403
- Baraffe, I. Charbrier, G. Allard, F. & Hauschildt, P. 2001, in *From Darkness to Light: Origin and Evolution of Young Stellar Clusters* ASP Conf. Series Vol. 243, 571, eds. T. Montmerle & P. André
- Barnes, P. J. Crutcher, R. M. Biegging, J. H. Storey, J. W. V. & Willner, S. P. 1989, ApJ, 342, 883
- Barrado y Navascués, D. et al. 2003, A&A, 404, 171
- Béjar, V. J. S. Zapatero Osorio, M. R. & Rebolo, R. 1999, ApJ, 521, 671
- Béjar, V. J. S. et al. 2001, ApJ, 556, 830
- Berriman, G. Reid, N. & Leggett, S. K. 1992, ApJ, 392, 31
- Bik, A. et al. 2003, A&A, 404, 249
- Binney, J. & Tremaine, S. 1987, *Galactic Dynamics* Princeton University Press (Princeton, New Jersey)
- Briceño, C. et al. 1997, AJ, 113, 740

- Briceño, C. et al. 2001, *Science*, 291, 93
- Briceño, C. et al. 2002, *ApJ*, 580, 317
- Blaauw, A. 1964, *ARA&A*, 2, 213
- Brown, A. G. A. de Geus, E. J. & deZeeuw, P. T. 1994, *A&A*, 289, 101
- Brown, A. G. A. Walter, F. M. & Blaauw, A. to be published in *The Orion Complex Revisited* eds. M. J. McCaughrean & A. Burkert (ASP)
- Burgasser, A. J. et al. 2004, *ApJ*, 604, 827
- Carpenter, J. M. , Hillenbrand, L. A. & Skrutskie, M. F. 2001, *AJ*, 121, 3160
- Carpenter, J. M. 2000, *AJ*, 120, 3139
- Comerón, F. Rieke, G. H. & Rieke, M. J. 1996 *ApJ*, 473, 294
- Dullemond, C. P. van den Ancker, M. E. Acke, B. & van Boekel, R. 2003, *ApJ*, 594, 47
- Duquennoy, A. & Mayor, M. 1991, *A&A*, 248, 485
- Feigelson, E. D. et al. 2003, *ApJ*, 584, 911
- Flaccomio, E. et al. 2003, *ApJ*, 582, 382
- Garmire, G. et al. 2000, *AJ*, 120, 1426
- Genzel, R. & Stutzki, J. 1989, *ARA&A*, 27, 41
- Gomez, M. & Lada, C. J. 1998 *ApJ*, 115, 1524
- Gullbring, E. Hartmann, L. Briceño, C. Calvet, N. & Muzerolle, J. 1998 *Cool Stars, Stellar Systems, and the Sun 10*, R. Donahue & J. Bookbinder (ASP: San Francisco)
- Herbig, G. H. 1977, *ApJ*, 214, 747
- Herbst, W. Herbst, D. K. Grossman, E. J. & Weinstein, D. 1994, *AJ*, 108, 1906
- Herbst, W. et al. 2002, *A&A*, 396, 513
- Hillenbrand, L. 1997, *AJ*, 113, 1733
- Hillenbrand, L. A. & Hartmann, L. W. 1998, *ApJ*, 492, 540
- Jayawardhana, R. Ardila, D. R. Stelzer, B. & Haisch, K. E. 2003, *AJ*, 126, 1515

- Jones, B. F. & Walker, M. F. 1988, AJ, 95, 1755
- Kenyon, S. J. & Hartmann, L. W. 1995, ApJS, 101, 117
- Kogure, T. et al. 1989, PASJ, 41 1195
- Kroupa, P. 2002, Science, 295, 82
- Lada, E. A. DePoy, D. L. Evans, N. J. & Gatley, I. 1991, ApJ, 371, 171
- Lada, C. J. & Lada, E. A. 2003 ARA&A, 41, 57
- Lampton, M. Margon, B. & Bowyer, S. 1976, ApJ, 208, 177
- Landolt, A. U. 1992, AJ, 104, 340
- Leggett, S. K. Allard, F., Geballe, T. R. Hauschildt, P. H. & Schweitzer, A. 2001, ApJ, 548, 908
- Leggett, S. K. et al. 2002, ApJ, 564, 452
- Lesh, J. R. 1968, ApJ, 152, 905
- Liu, W. M. Meyer, M. R. Cotera, A. S. & Young, E. T. 2003 AJ, 126, 1665
- Luhman, K. 1999, ApJ, 525, 466
- Markwardt, C. B. 2002, <http://astrog.physics.wisc.edu/~craigm/idl/idl.html>
- Martín, E. L. & Zapatero Osorio, M. R. 2003, ApJ, 593, L113
- Meyer, M. 1996, Ph. D. thesis, Univ. Massachusetts, Amherst
- Mink, D. J. 1997, in *Astronomical Data Analysis Software and Systems VI*, A. S. P. Conference Series, Vol. 125, G. Hunt and H. E. Payne, eds. p. 249
- Monet, D. et al. 1998, The USNO-A2.0 Catalogue, (U. S. Naval Observatory, Washington DC)
- O'Dell, C. R. 2001, ARA&A, 39, 99
- Oliveira, J. M. Jeffries, R. D. van Loon J. Th. & Kenyon, M. J. 2004, MNRAS, 347, 1327
- Perrin, G. et al. 1998, A&A, 331, 619
- Perryman, M. A. C. et al. A&A, 323, 49

- Rebull, L. M. 2001, *AJ*, 121, 1676
- Sagar, R. & Richtler, T. 1991 *A&A*, 250, 324
- Scally, A. Clarke, C. & McCaughrean, M. J. 1999, *MNRAS*, 306, 253
- Sherry, W. H. 2003, *The Young Low-Mass Population of Orion's Belt*, Ph. D. Thesis, State University of New York, Stony Brook
- Sherry, W. H. Walter, F. M. & Wolk, S. J. in preparation
- Simon, M. Close, L. M. & Beck, T. L. 1999, *AJ*, 117, 1375
- Simon, M. Dutry, A. & Guilloteau, S. 2000, *ApJ*, 545, 1034
- Stassun, K. G. Mathieu, R. D. Mazeh, T. & Vrba, F. J. 1999, *AJ*, 117, 2941
- Sterzik, M. F. Alcalá, J. M. Neuhäuser, R. and Schmitt, J. H. M. M. 1995, *A&A*297, 418
- Sterzik, M. F. Alcalá, J. M. Neuhäuser, R. and Durisen, R. H. 2004, to be published in *The Orion Complex Revisited* eds. M. J. McCaughrean & A. Burkert (ASP)
- Torres, G. & Rebas, I. 2002, *ApJ*, 567, 1140
- van Altena, W. F. 1988, *AJ*, 95, 1714
- Walter, F. M. et al. 1994, *AJ*, 107, 692
- Walter, F. M. Wolk, S. J. & Sherry, W. H. 1998, *Cool Stars, Stellar Systems, and the Sun 10*, R. Donahue & J. Bookbinder (ASP: San Francisco)
- Walter, F. M. Alcalá, J. M. Neuhäuser, R. Sterzik, M. & Wolk, S. J. 2000, *Protostars and Planets IV*, V. Mannings, A. P. Boss, and S. S. Russell, (Tucson: University of Arizona), p. 273
- Warren, W. H. Jr. & Hesser, J. E. 1977a, *ApJS*, 34, 115
- Warren, W. H. Jr. & Hesser, J. E. 1977b, *ApJS*, 34, 207
- Warren, W. H. Jr. & Hesser, J. E. 1978, *ApJS*, 36, 497
- White, R. J. et al. 1999, *ApJ*, 520, 811
- Wiramihardja, S. D. et al. 1989, *PASJ*, 41, 155
- Wiramihardja, S. D. 1991, *PASJ*, 43, 27

Wiramihardja, S. D. 1993, PASJ, 45, 634

Wolk, S. J. 1996, *Watching the Stars go 'Round and 'Round*, PhD Thesis, State University of New York, Stony Brook

Zapatero Osorio, M. R. et al. 2000, Science, 290, 103

Zapatero Osorio, M. R. et al. 2002a, A&A, 384, 937

Zapatero Osorio, M. R. et al. 2002b, ApJ, 578, 536

deZeeuw, P. T. et al. 1999, AJ, 117, 354

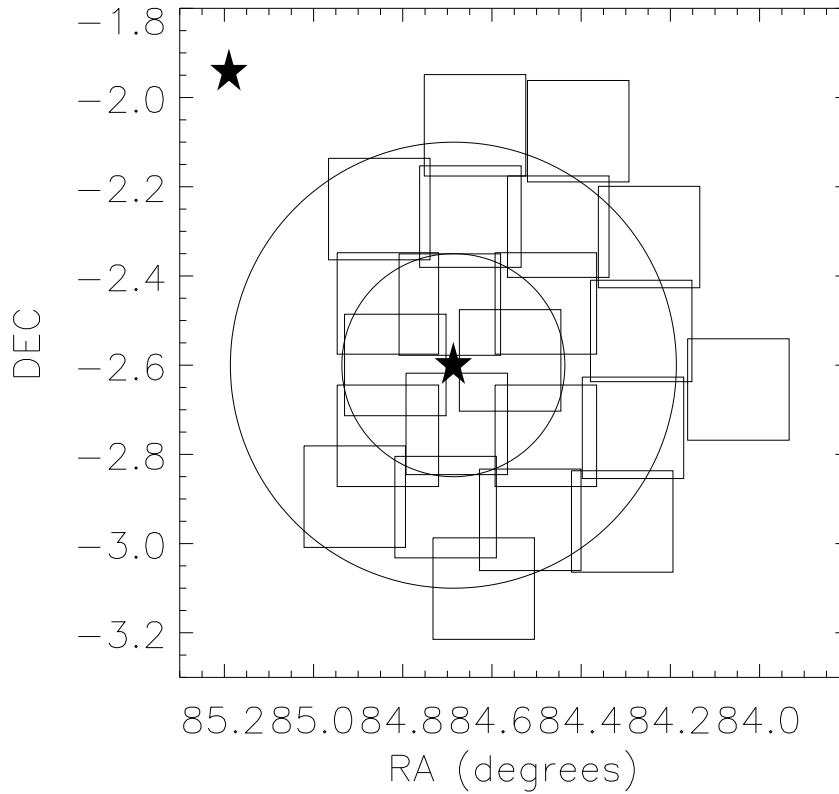


Fig. 1.— This figure shows the positions of our σ Ori survey fields. The stars mark the positions of σ Ori and ζ Ori. The circles mark radii of 0.25° and 0.5° from σ Ori. The four fields immediately around σ Ori were from Wolk (1996). The other four fields which lie partially within the inner 0.25° are the fields from the 1998 CTIO 1.5m run. All the other fields were observed during our 1998 CTIO 0.9m run.

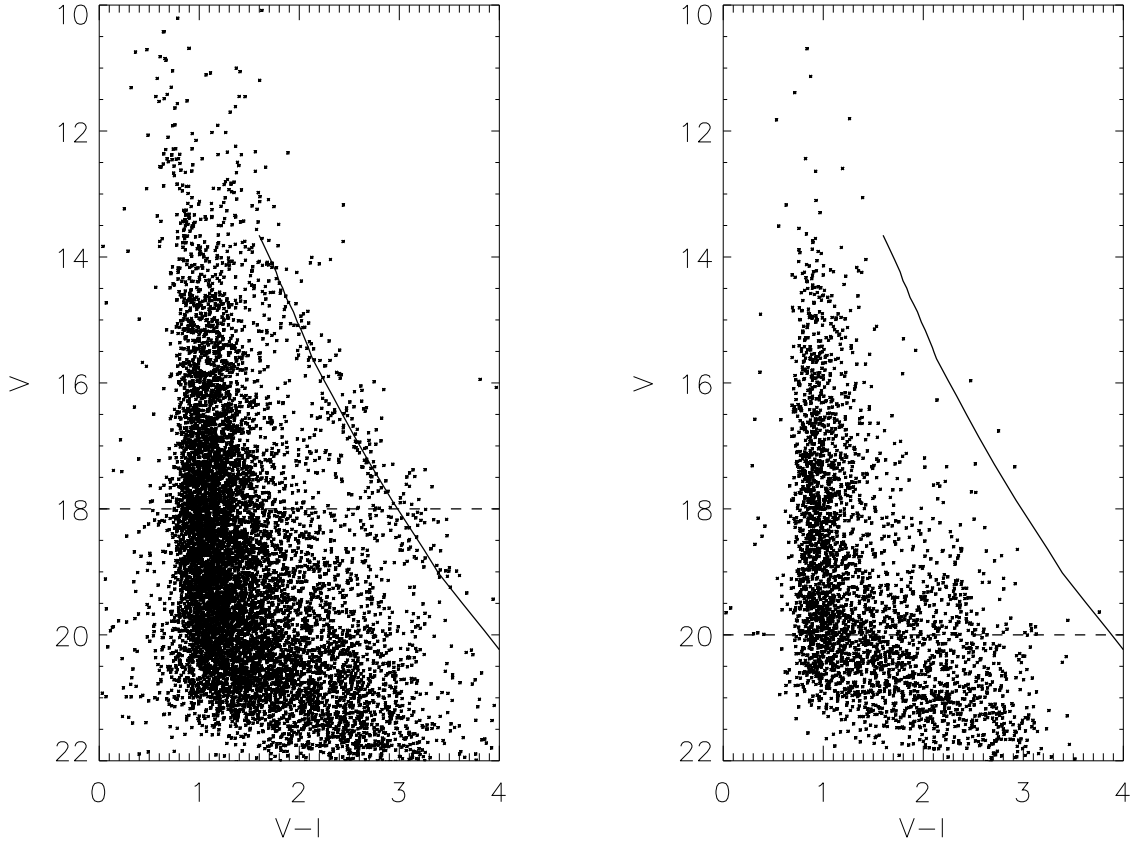


Fig. 2.— The left panel shows the V vs. $V-I_C$ color-magnitude diagram of 9556 stars in 0.89 deg^2 around σ Ori. The solid line is a 2.5 Myr isochrone (Baraffe et al. 1998; Baraffe et al. 2001) at a distance of 440 pc (Brown et al. in press). This isochrone marks the expected position of the PMS locus for Orion OB1b. There is a clear increase in the density of stars around the expected position of the PMS locus. The completeness limit of these data is marked by the dashed line. The right panel shows the same CMD for our 0.27 deg^2 control fields. The isochrone (solid line) is the same as in the left panel. The dashed line marks the fainter completeness limit of the control fields.

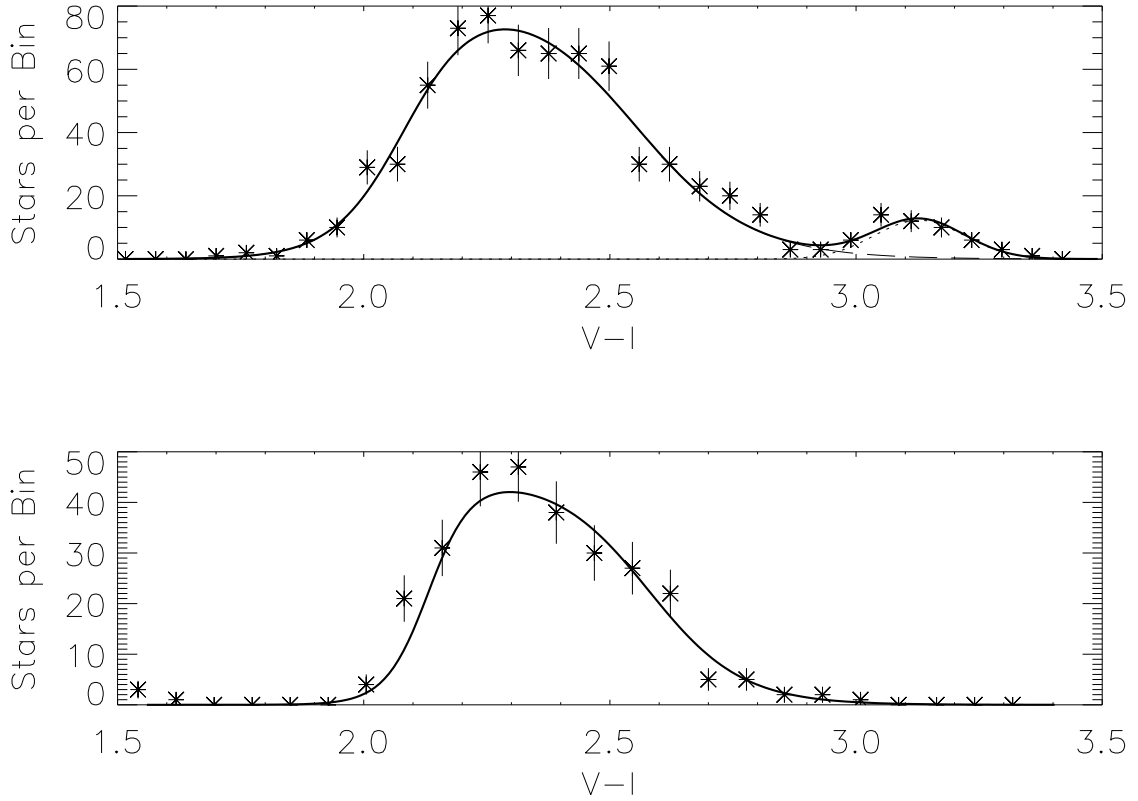


Fig. 3.— The upper panel shows one of the five independent cross-section through the σ Ori CMD (left panel of Figure 2). The solid line is the fit to the distribution of stars along the cross-section. The Gaussian component of the fit is marked by a dotted line which is mostly obscured by the solid line. The fit to the field star distribution is marked by a dashed line. The lower panel shows the equivalent cross-section through the CMD of our control field (right panel of Figure 2). There is a clear excess of stars around $V-I=3.1$ in the σ Ori cross-section that is absent in the control field cross-section.

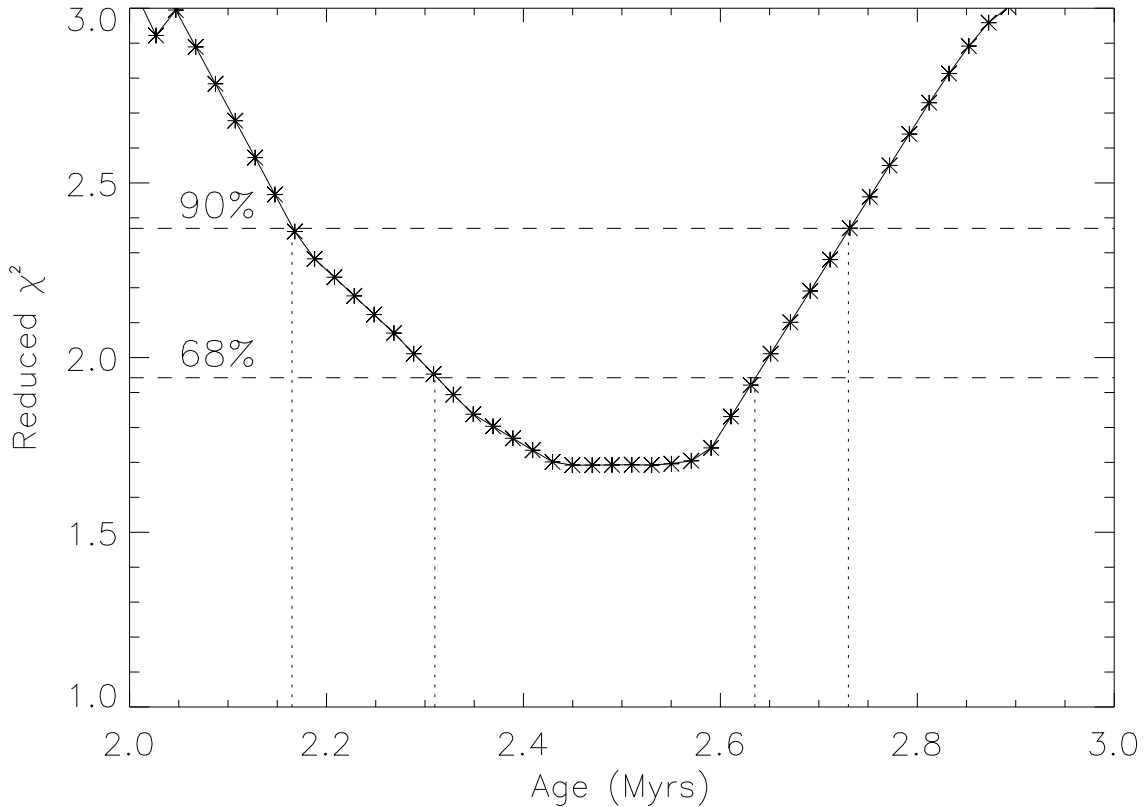


Fig. 4.— We estimated the uncertainty in the cluster age from this distribution of reduced χ^2 . The dashed horizontal lines mark the 68% and 90% confidence intervals. The dotted vertical lines mark the ages which bound these confidence intervals. The cluster age lies between 2.31 Myrs and 2.64 Myrs (68% confidence), or 2.17 Myrs and 2.73 Myrs (90% confidence). At the 99% confidence interval (not marked) the cluster age lies between 2.0 Myrs and 3.0 Myrs. The best fit age based on the five independent cross-sections is 2.45 ± 0.3 Myr (90% confidence).

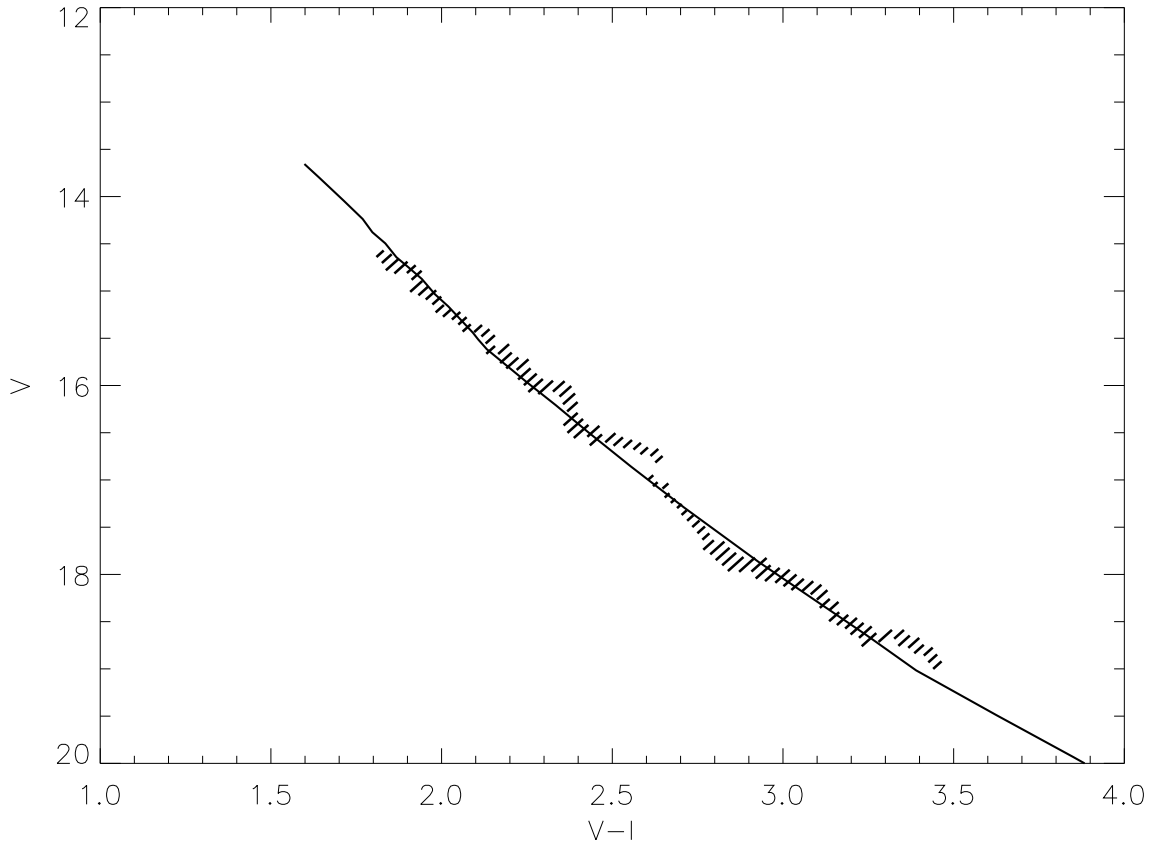


Fig. 5.— The best fit center of the PMS locus for each cross-section is marked by short diagonal lines which extend $\pm 1\sigma$ around the best fit center of the PMS locus. The long line is the best-fit 2.5 Myr isochrone (Baraffe et al. 1998; 2001). The combination of our adopted color-temperature relation from Table 3 and the Lyon group isochrone is a good match for the center of the PMS locus.

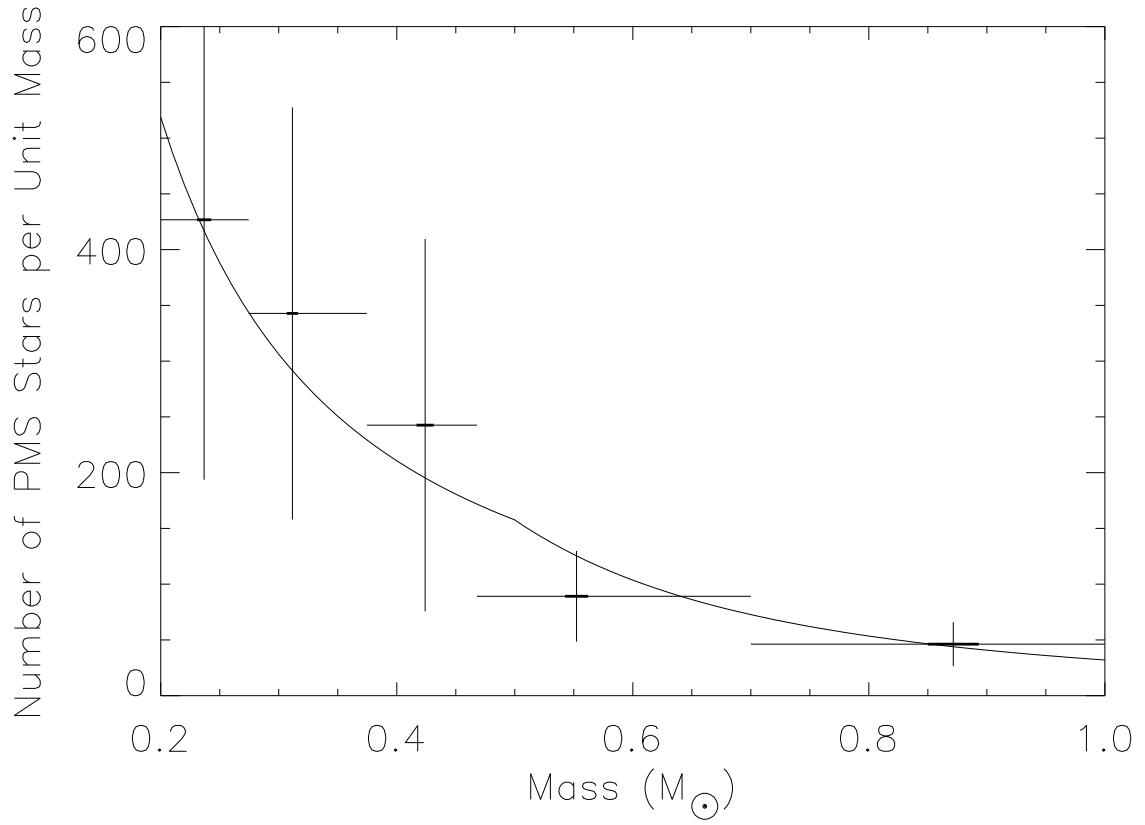


Fig. 6.— This plot shows the number of stars per unit mass from five independent cross-sections through the CMD. The observed IMF is consistent with the field star IMF of Kroupa (2002), shown as a solid line.

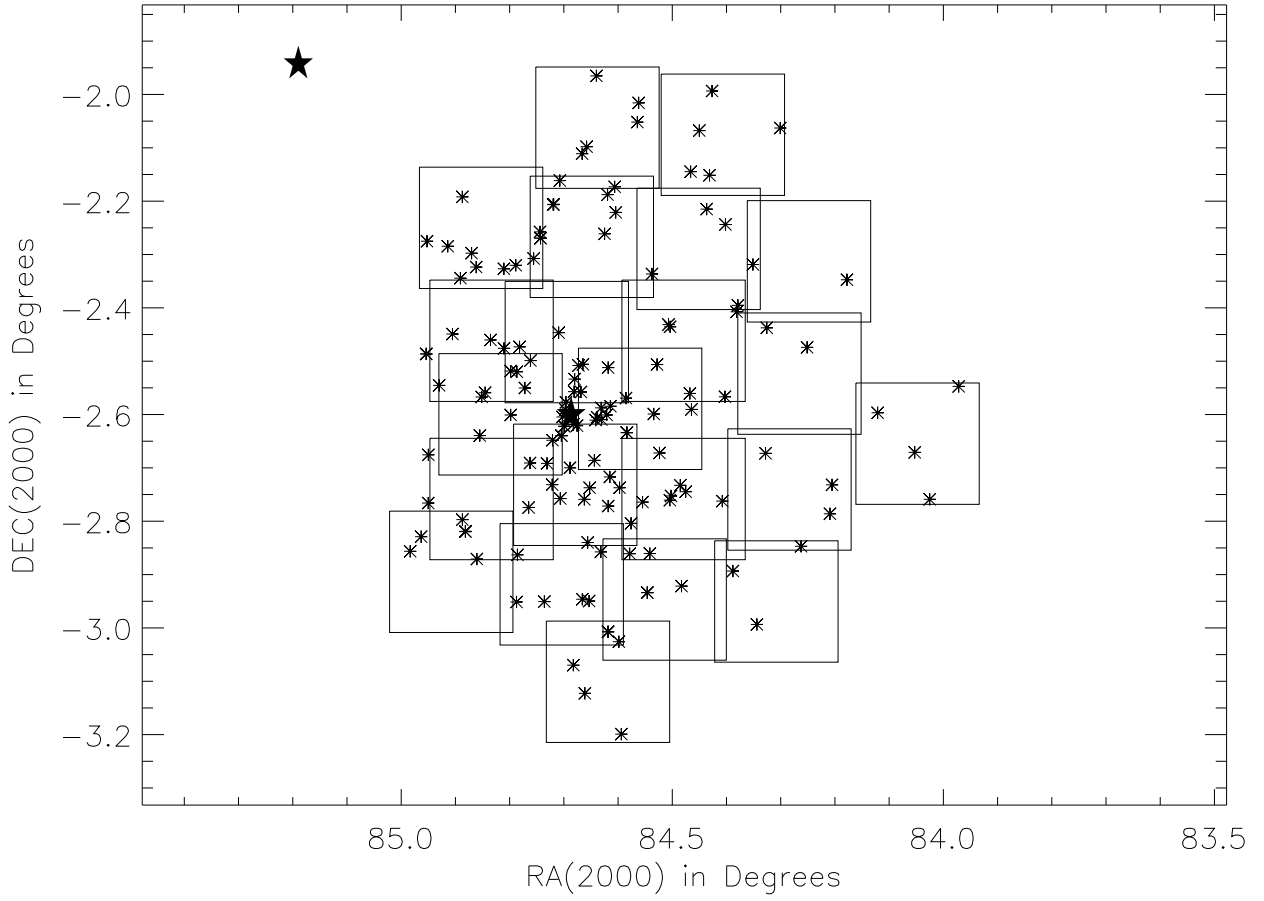


Fig. 7.— This plot shows the spatial distribution of likely PMS stars ($P_{PMS} \geq 40\%$) near σ Ori. The two large star symbols are σ Ori and ζ Ori. There is a very clear concentration of PMS stars around σ Ori. The boxes are the boundaries of our 0.9m fields.

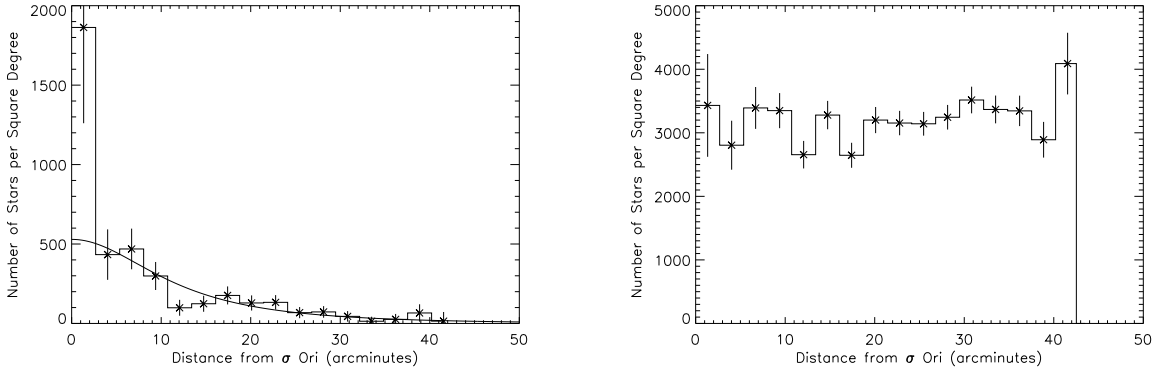


Fig. 8.— This left panel shows the radial profile of likely PMS stars near σ Ori ($\text{Prob}_{PMS} \geq 40\%$). The density of field stars (50 deg^{-2} in the PMS locus) has been subtracted off. The error bars are the square root of the number of stars per bin. The solid curve is a King model with $\frac{\psi(0)}{\sigma} = 5.0$, $c = 1.1$, a central density of $\sim 3 \text{ stars pc}^{-3}$, a King radius of 1.6 pc, and a tidal radius of $\sim 20 \text{ pc}$. The reduced χ^2 is 0.9. The right panel shows the radial profile of field stars ($P_{PMS} < 1\%$) near σ Ori. There is no concentration of field stars around σ Ori. A 2 sided KS test shows that the two distributions are different at a 99.9% confidence level.

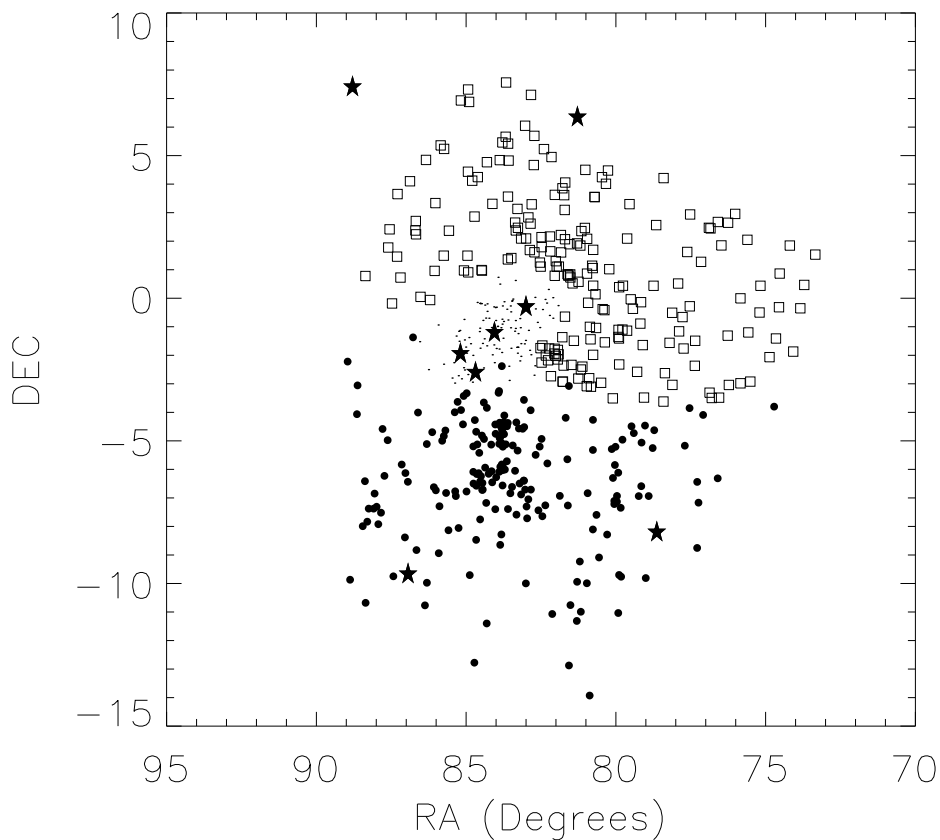


Fig. 9.— This plot shows the members of the Orion OB1 sub-associations as assigned by Brown, de Geus, & de Zeeuw (1994). These are mainly O and B stars with just a few A and F stars. The three belt stars, δ Ori, ϵ Ori, and ζ Ori, as well as σ Ori are members of Orion OB1b which have been marked by large stars. Betelgeuse, Saiph, Rigel, and Bellatrix, the four bright stars which mark shoulders and knees of Orion, are also marked with large stars. These stars are not members of the Orion OB1 association, but make it easier to visualize the scale of the association on the night sky. Stars assigned to Orion OB1a are marked with open squares. B stars which have been assigned to Orion OB1b are marked by small dots. Stars assigned to Orion OB1c are marked by filled circles.

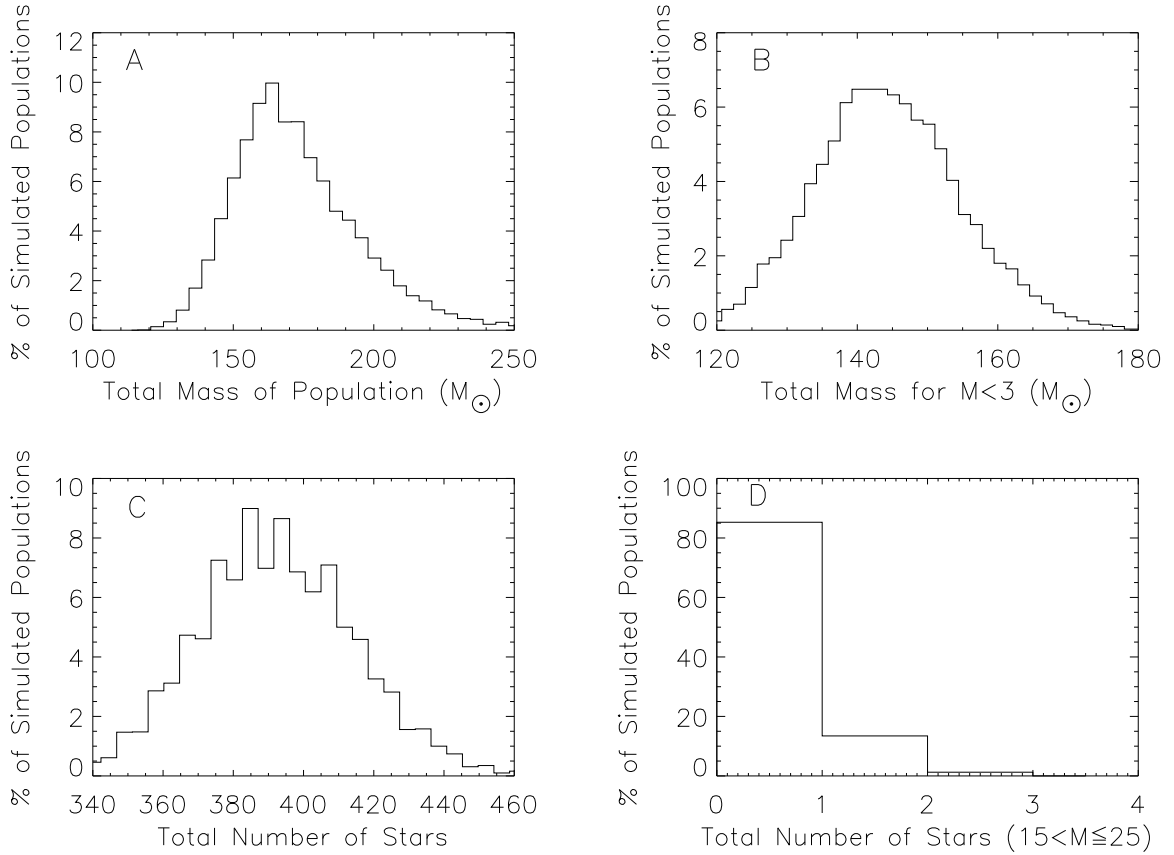


Fig. 10.— These are the results of a Monte Carlo simulation of 10,000 stellar populations which each have 160 primaries with masses in the range $0.2 \leq M \leq 1.0 M_{\odot}$. Panel A shows the distribution of simulations as a function of the total mass of the simulated population. Panel B shows the distribution of simulations as a function of the mass in stars that have masses less than $3 M_{\odot}$. Panel C shows the distribution of simulated populations as a function of the number of stars making up the population. Panel D shows the fraction of simulations which have a given number of stars with masses in the range $15 < M \leq 25 M_{\odot}$.

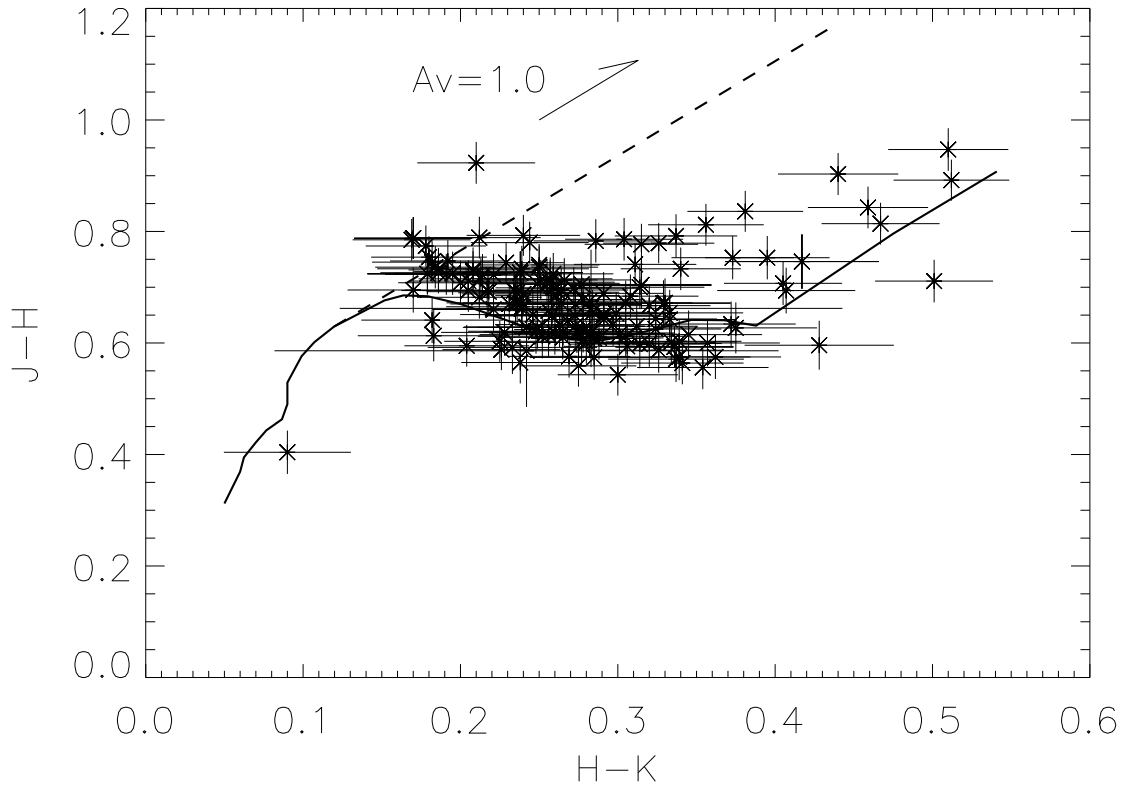


Fig. 11.— The $J-H$ vs. $H-K$ color-color diagram of 164 stars with $P_{mem} \geq 50\%$. The data are from the 2MASS catalog. The solid line marks the position of main sequence. The arrow shows the $A_V=1.0$ reddening vector. Any reddened main sequence or giant stars should lie to the right of the dashed line.

Table 1. Log of Observing Runs

Telescope	Filters	Completeness at V	Dates
CTIO 0.9m	VRI	18.5	Jan 29, 1996
CTIO 1.5m	BVRI	18.0	Dec 3, 1998
CTIO 0.9m	BVRI	20.0	Dec 7-11, 1998
CTIO 0.9m	BVRI	20.0	Jan 4-9, 2002

Table 2. Description of the Parameters in the CMD Cross-Section Fit

Parameter	Distribution	Purpose
N_f	field	Normalization of the field star dist.
a	field	Sets the blue slope of the field dist.
μ_1	field	Sets the position of the rising exponential
b	field	Sets the position of the falling exponential
μ_2	field	Helps fix the position and width of the field dist.
N_p	PMS	Normalization of the Gaussian
μ_p	PMS	V-I of the center of the Gaussian
σ	PMS	Sets the full width at half maximum

Table 3. Adopted Color-Temperature Relation for ~ 3 Myr Old Stars.

Sp. Type	T_{eff}^a	BC ^b	U–V	B–V	V–R _C	V–I _C	V–J	V–H	V–K	V–L
B0	30000	–3.16	–1.38	–0.30	–0.11	–0.26	–0.70	–0.81	–0.93	–0.99
B1	25400	–2.70	–1.23	–0.26	–0.10	–0.22	–0.61	–0.71	–0.81	–0.86
B2	22000	–2.35	–1.08	–0.22	–0.09	–0.19	–0.55	–0.65	–0.74	–0.77
B3	18700	–1.94	–0.94	–0.19	–0.07	–0.16	–0.45	–0.53	–0.61	–0.63
B4	17000	–1.70	–0.84	–0.16	–0.05	–0.13	–0.40	–0.47	–0.55	–0.55
B5	15400	–1.46	–0.72	–0.14	–0.03	–0.10	–0.35	–0.41	–0.57	–0.48
B6	14000	–1.21	–0.61	–0.13	–0.03	–0.09	–0.32	–0.37	–0.43	–0.45
B7	13000	–1.02	–0.50	–0.11	–0.02	–0.08	–0.29	–0.34	–0.39	–0.42
B8	11900	–0.80	–0.40	–0.09	–0.02	–0.15	–0.26	–0.31	–0.35	–0.39
B9	10500	–0.51	–0.17	–0.06	–0.01	–0.08	–0.14	–0.16	–0.18	–0.20
A0	9520	–0.30	0.00	0.00	0.00	0.00	0.00	0.00	0.00	0.00
A1	9230	–0.23	0.05	0.03	0.01	0.02	0.06	0.06	0.07	0.08
A2	8970	–0.20	0.10	0.06	0.02	0.05	0.12	0.13	0.14	0.15
A3	8720	–0.17	0.15	0.09	0.03	0.08	0.18	0.21	0.22	0.23
A4	8460	–0.16	0.20	0.12	0.04	0.11	0.25	0.28	0.30	0.31
A5	8200	–0.15	0.24	0.14	0.06	0.14	0.30	0.36	0.38	0.40
A6	8050	–0.13	0.26	0.16	0.08	0.21	0.34	0.41	0.44	0.47
A7	7850	–0.12	0.28	0.19	0.10	0.27	0.39	0.47	0.50	0.53
A8	7580	–0.10	0.30	0.23	0.13	0.32	0.45	0.54	0.57	0.60
A9	7390	–0.10	0.32	0.27	0.16	0.37	0.50	0.61	0.64	0.67
F0	7200	–0.09	0.34	0.31	0.20	0.42	0.54	0.67	0.70	0.73
F1	7050	–0.10	0.36	0.33	0.22	0.44	0.58	0.73	0.76	0.79
F2	6890	–0.11	0.37	0.35	0.23	0.46	0.63	0.79	0.82	0.85
F3	6740	–0.12	0.38	0.37	0.24	0.48	0.69	0.87	0.91	0.94
F4	6590	–0.13	0.39	0.39	0.26	0.51	0.76	0.97	1.01	1.05
F5	6440	–0.14	0.40	0.42	0.27	0.54	0.83	1.06	1.10	1.14
F6	6360	–0.15	0.44	0.46	0.29	0.58	0.87	1.17	1.21	1.25
F7	6280	–0.16	0.49	0.50	0.31	0.62	0.98	1.27	1.32	1.36
F8	6200	–0.16	0.54	0.52	0.33	0.66	1.00	1.30	1.35	1.39
F9	6115	–0.17	0.59	0.55	0.34	0.69	1.03	1.33	1.38	1.43
G0	6030	–0.18	0.64	0.58	0.35	0.71	1.05	1.36	1.41	1.46
G1	5945	–0.19	0.64	0.60	0.36	0.72	1.08	1.39	1.44	1.49
G2	5860	–0.20	0.64	0.62	0.37	0.73	1.09	1.41	1.46	1.51
G3	5830	–0.20	0.71	0.63	0.38	0.74	1.11	1.44	1.49	1.54
G4	5800	–0.21	0.79	0.64	0.39	0.75	1.15	1.47	1.53	1.58
G5	5770	–0.21	0.86	0.66	0.39	0.76	1.16	1.52	1.58	1.63
G6	5700	–0.22	0.90	0.68	0.40	0.77	1.18	1.58	1.64	1.69
G7	5630	–0.23	0.95	0.71	0.41	0.79	1.27	1.66	1.72	1.77
G8	5520	–0.25	1.00	0.73	0.42	0.81	1.28	1.69	1.76	1.81
G9	5410	–0.28	1.13	0.78	0.44	0.83	1.30	1.73	1.80	1.86
K0	5250	–0.31	1.27	0.82	0.46	0.85	1.43	1.88	1.96	2.02
K1	5080	–0.37	1.44	0.85	0.50	0.93	1.53	2.00	2.09	2.15
K2	4900	–0.42	1.52	0.89	0.54	1.01	1.63	2.13	2.22	2.29
K3	4730	–0.50	1.80	0.97	0.58	1.08	1.79	2.33	2.42	2.51
K4	4590	–0.55	2.01	1.07	0.65	1.15	1.95	2.53	2.63	2.73
K5	4350	–0.72	2.22	1.16	0.73	1.36	2.13	2.74	2.85	2.96

Table 3—Continued

Sp. Type	T_{eff}^a	BC ^b	U–V	B–V	V–R _C	V–I _C	V–J	V–H	V–K	V–L
K7	4060	–0.92	2.64	1.38	0.84	1.60	2.37	3.03	3.16	3.27
M0	3850	–1.25	2.66	1.41	0.91	1.80	2.79	3.48	3.65	3.79
M1	3705	–1.43	2.74	1.48	0.94	1.96	3.00	3.67	3.87	4.02
M2	3560	–1.64	2.69	1.52	0.98	2.14	3.24	3.91	4.11	4.27
M3	3415	–2.03	2.65	1.55	1.10	2.47	3.78	4.40	4.65	4.85
M4	3270	–2.56	2.89	1.60	1.23	2.86	4.38	4.98	5.26	5.49
M5	3125	–3.29	3.07	1.82	1.50	3.40	5.18	5.80	6.12	6.41
M6	2990	–4.35	3.33	2.00	2.00	4.30	6.27	6.93	7.30	7.66
M7	2890	–4.53	3.50	2.05	2.00	4.45	6.59	7.17	7.53	8.11
M9	2550	–5.70	...	2.10	2.10	4.55	7.58	8.38	8.86	9.61
L0	2200	–6.10	4.66	8.11	8.88	9.32	10.0
L2	2100	–6.70	4.84	8.49	9.41	9.96	11.0

^a T_{eff} for M stars are from Luhman (1999).

^bColors and bolometric correction for stars earlier than M7 were taken from Kenyon & Hartmann (1995). For stars later than M7 we used U–V, B–V, and V–R_C from Berriman et al. (1992) and V–I_C, V–J, V–H, V–K, V–L and bolometric corrections from Leggett et al. (2001).

Table 4. Photometry of Likely Cluster Members

RA(2000)	DEC(2000)	B	Err	V	Err	R	Err	I	Err	J ^a	Err	H ^a	Err	K ^a	Err	P	M ^b
05:39:40.974	-02:16:24.23	19.37	0.03	18.01	0.02	16.54	0.02	14.75	0.02	12.91	0.03	12.16	0.03	11.76	0.03	98	0.20
05:38:43.751	-02:52:42.71	19.59	0.04	18.07	0.02	16.63	0.02	14.86	0.02	13.03	0.03	12.39	0.03	12.10	0.03	98	0.20
05:38:23.563	-02:41:31.68	18.26	0.39	16.91	0.05	15.08	0.02	13.30	0.03	12.74	0.03	12.40	0.03	98	0.21
05:38:36.759	-02:36:43.68	18.18	0.11	16.71	0.12	14.97	0.04	13.05	0.03	12.46	0.03	12.12	0.03	97	0.20
05:38:17.794	-02:40:50.02	19.72	0.20	18.14	0.08	16.81	0.04	14.98	0.02	13.20	0.03	12.59	0.03	12.25	0.03	97	0.21
05:39:46.607	-02:26:31.21	19.65	0.18	18.05	0.07	16.65	0.03	14.87	0.01	13.01	0.03	12.36	0.03	12.06	0.03	96	0.21
05:39:25.608	-02:34:04.04	20.12	0.32	18.22	0.08	16.71	0.04	14.96	0.02	13.20	0.03	12.55	0.03	12.27	0.05	96	0.20
05:38:17.467	-02:09:23.58	19.64	0.05	18.10	0.01	16.70	0.01	14.96	0.01	13.30	0.03	12.66	0.03	12.37	0.03	95	0.22
05:37:55.113	-02:27:36.11	20.55	0.44	18.49	0.10	17.18	0.07	15.38	0.02	13.59	0.03	12.96	0.03	12.72	0.03	95	0.22
05:38:54.916	-02:28:58.24	19.84	0.21	18.61	0.10	17.26	0.06	15.50	0.02	13.79	0.03	13.19	0.03	12.85	0.03	94	0.22
05:38:37.446	-02:50:23.71	19.33	0.04	17.85	0.02	16.43	0.02	14.66	0.02	12.84	0.03	12.20	0.03	11.93	0.03	94	0.21
05:38:16.019	-02:38:05.03	18.30	0.11	16.81	0.12	15.20	0.03	13.60	0.03	12.89	0.03	12.62	0.03	94	0.22
05:36:46.923	-02:33:28.20	20.07	0.06	18.45	0.02	17.02	0.02	15.27	0.02	13.57	0.03	12.99	0.03	12.66	0.03	94	0.21
05:36:02.373	-02:36:27.74	20.07	0.07	18.51	0.02	17.11	0.01	15.41	0.01	13.78	0.03	13.15	0.04	12.78	0.04	94	0.22
05:38:43.790	-02:37:07.05	17.93	0.08	16.59	0.09	14.80	0.04	93	0.22
05:38:36.589	-02:44:13.89	17.65	0.06	16.08	0.07	14.32	0.02	12.56	0.03	11.91	0.03	11.62	0.03	93	0.19
05:37:48.470	-02:09:06.29	20.07	0.06	18.64	0.02	17.25	0.01	15.54	0.01	13.90	0.03	13.21	0.03	12.80	0.03	93	0.22
05:38:49.920	-02:37:35.72	18.17	0.11	16.52	0.12	14.83	0.03	13.05	0.03	12.37	0.03	12.11	0.03	92	0.18
05:37:40.600	-02:08:57.56	19.35	0.03	18.09	0.01	16.74	0.01	15.00	0.01	92	0.23
05:39:31.594	-02:49:08.10	18.52	0.06	16.94	0.02	15.76	0.02	14.34	0.01	91	0.33
05:37:18.713	-02:40:21.78	16.87	0.02	15.38	0.02	14.33	0.02	13.26	0.02	12.21	0.03	11.61	0.03	11.26	0.03	91	0.58
05:37:11.681	-02:31:56.42	19.88	0.05	18.30	0.02	16.94	0.02	15.23	0.02	13.53	0.03	12.87	0.03	12.63	0.03	91	0.23
05:39:51.161	-02:49:44.36	18.26	0.01	16.74	0.01	15.60	0.01	14.16	0.01	12.81	0.03	12.13	0.03	11.92	0.03	90	0.34
05:39:31.526	-02:49:10.28	18.62	0.07	17.03	0.02	15.85	0.02	14.36	0.01	90	0.31
05:38:41.500	-02:30:29.00	17.04	0.04	15.84	0.08	14.39	0.03	12.86	0.03	12.15	0.03	11.94	0.03	90	0.32
05:38:21.194	-02:54:11.03	19.60	0.05	18.21	0.02	16.68	0.02	14.82	0.02	12.96	0.03	12.25	0.03	11.85	0.03	90	0.17
05:38:01.663	-02:25:52.66	18.71	0.07	17.21	0.03	16.01	0.02	14.54	0.01	13.01	0.03	12.33	0.03	12.06	0.03	90	0.31
05:39:02.775	-02:29:55.78	18.42	0.06	16.91	0.02	15.72	0.01	14.21	0.01	12.63	0.03	12.01	0.03	11.71	0.03	89	0.30
05:38:47.079	-02:34:36.77	17.36	0.09	16.09	0.10	14.64	0.04	89	0.30
05:38:39.902	-02:06:39.72	18.85	0.02	17.27	0.01	16.08	0.01	14.60	0.01	13.16	0.03	12.55	0.03	12.29	0.03	89	0.31
05:38:38.929	-02:45:32.39	17.26	0.04	15.92	0.05	14.58	0.02	12.94	0.03	12.20	0.03	11.89	0.03	89	0.31
05:39:47.990	-02:40:31.97	17.86	0.04	16.38	0.01	15.23	0.01	13.83	0.01	12.45	0.03	11.66	0.03	11.45	0.03	88	0.35
05:39:39.376	-02:17:04.38	16.95	0.02	15.35	0.02	14.29	0.02	13.24	0.02	11.67	0.03	10.72	0.03	10.21	0.03	88	0.61
05:38:56.630	-02:57:02.20	16.92	0.02	15.46	0.02	14.44	0.02	13.32	0.02	12.10	0.03	11.54	0.03	11.30	0.03	88	0.56
05:38:48.590	-02:36:16.10	15.45	0.10	14.24	0.12	13.37	0.06	88	0.64

Table 4—Continued

RA(2000)	DEC(2000)	B	Err	V	Err	R	Err	I	Err	J ^a	Err	H ^a	Err	K ^a	Err	P	M ^b
05:38:43.449	-02:33:25.33	15.12	0.01	14.15	0.02	13.09	0.01	88	0.68
05:38:40.078	-02:50:37.14	20.15	0.08	18.66	0.02	17.26	0.02	15.48	0.02	13.68	0.03	13.07	0.03	12.81	0.03	88	0.21
05:38:23.637	-03:01:33.22	18.08	0.02	16.57	0.02	15.42	0.02	14.04	0.02	12.76	0.03	12.14	0.03	11.91	0.03	88	0.36
05:38:18.865	-02:51:39.07	18.20	0.05	16.81	0.02	15.65	0.01	14.25	0.01	12.83	0.03	12.05	0.03	11.74	0.03	88	0.35
05:38:18.246	-02:48:14.33	18.14	0.05	16.68	0.02	15.54	0.01	14.15	0.01	12.78	0.03	12.03	0.03	11.80	0.03	88	0.36
05:38:08.179	-02:35:56.24	16.19	0.02	15.08	0.02	13.76	0.01	12.17	0.03	11.39	0.03	11.08	0.03	88	0.40
05:37:48.019	-02:04:03.72	17.84	0.01	16.45	0.01	15.26	0.01	13.79	0.01	12.20	0.03	11.46	0.03	11.27	0.03	88	0.32
05:37:03.006	-02:50:49.09	18.61	0.02	17.23	0.01	16.04	0.01	14.58	0.01	13.02	0.03	12.35	0.03	12.02	0.03	88	0.32
05:39:49.442	-02:23:45.86	20.21	0.35	18.15	0.07	16.86	0.04	15.12	0.02	13.44	0.03	12.75	0.03	12.45	0.03	87	0.23
05:39:26.768	-02:42:58.25	21.49	1.12	18.90	0.13	17.25	0.06	15.52	0.03	13.19	0.03	12.40	0.03	12.12	0.03	87	0.18
05:38:58.552	-02:15:27.54	17.90	0.02	16.44	0.02	15.30	0.02	13.97	0.02	12.51	0.03	11.79	0.03	11.54	0.03	87	0.38
05:38:53.162	-02:43:53.05	17.00	0.01	15.60	0.01	14.57	0.01	13.49	0.01	12.23	0.03	11.50	0.03	11.29	0.03	87	0.61
05:38:42.160	-02:37:15.16	15.12	0.01	14.04	0.03	13.06	0.02	11.80	0.03	11.01	0.03	10.77	0.03	87	0.66
05:38:31.479	-02:35:14.93	15.64	0.01	14.60	0.03	13.49	0.01	11.52	0.03	10.71	0.03	10.35	0.03	87	0.56
05:38:31.329	-02:36:34.00	16.30	0.02	15.09	0.02	13.80	0.01	12.19	0.03	11.47	0.03	10.97	0.03	87	0.37
05:38:23.609	-02:20:47.87	19.81	0.09	18.64	0.03	17.14	0.03	15.32	0.03	13.42	0.03	12.80	0.03	12.47	0.03	87	0.19
05:38:09.944	-02:51:37.73	17.81	0.03	16.40	0.02	15.25	0.01	13.93	0.01	12.36	0.03	11.58	0.03	11.25	0.03	87	0.38
05:37:58.401	-02:41:26.16	21.06	0.84	18.63	0.11	17.26	0.06	15.31	0.02	13.28	0.03	12.70	0.03	12.43	0.03	87	0.19
05:37:50.332	-02:12:24.54	20.25	0.13	18.56	0.03	17.20	0.03	15.53	0.03	13.91	0.03	13.30	0.03	13.04	0.03	87	0.23
05:37:30.958	-02:23:43.08	18.33	0.03	17.11	0.03	15.91	0.03	14.51	0.03	13.03	0.03	12.40	0.03	12.09	0.03	87	0.34
05:37:18.167	-02:26:14.92	18.81	0.02	17.25	0.02	16.01	0.02	14.51	0.02	13.07	0.03	12.47	0.03	12.20	0.03	87	0.29
05:35:53.226	-02:32:50.08	17.99	0.01	16.52	0.01	15.38	0.01	14.04	0.01	12.63	0.03	11.94	0.03	11.72	0.03	87	0.38
05:40:06.707	-02:57:38.98	20.16	0.07	18.67	0.02	17.13	0.01	15.25	0.01	13.67	0.03	13.07	0.03	12.64	0.04	86	0.17
05:39:26.494	-02:52:15.32	18.91	0.09	17.33	0.03	16.09	0.02	14.58	0.01	13.03	0.03	12.33	0.03	12.08	0.03	86	0.29
05:39:20.254	-02:38:25.93	21.12	0.78	18.97	0.15	17.57	0.09	15.56	0.03	13.62	0.03	13.05	0.03	12.77	0.03	86	0.17
05:39:08.542	-02:51:46.72	16.64	0.01	15.23	0.01	14.21	0.01	13.23	0.01	11.99	0.03	11.22	0.03	11.04	0.03	86	0.73
05:39:01.365	-02:18:27.17	16.28	0.02	15.01	0.02	14.02	0.02	12.99	0.02	11.74	0.03	10.85	0.03	10.34	0.03	86	0.70
05:38:52.714	-2:12:23.60	17.92	0.03	16.41	0.03	15.23	0.03	13.77	0.03	86	0.32
05:38:43.792	-03:04:11.46	18.99	0.02	17.45	0.01	16.21	0.01	14.68	0.01	12.96	0.03	12.23	0.03	11.89	0.03	86	0.29
05:38:36.818	-02:56:58.56	18.01	0.02	16.49	0.02	15.34	0.02	14.04	0.02	12.63	0.03	11.89	0.03	11.64	0.03	86	0.39
05:38:33.980	-02:36:37.74	16.39	0.02	15.24	0.02	13.72	0.01	86	0.31
05:38:27.400	-02:35:04.25	17.09	0.04	15.84	0.08	14.38	0.03	12.81	0.03	12.13	0.03	11.84	0.03	86	0.30
05:37:54.070	-02:44:40.58	18.58	0.07	17.07	0.03	15.90	0.02	14.48	0.01	13.02	0.03	12.33	0.03	12.09	0.03	86	0.34
05:39:32.908	-02:47:49.09	16.50	0.01	15.09	0.01	14.09	0.01	13.10	0.01	11.84	0.03	11.13	0.03	10.93	0.03	85	0.75
05:39:08.936	-02:57:04.91	18.94	0.03	17.48	0.02	16.26	0.02	14.76	0.02	13.29	0.03	12.59	0.03	12.32	0.03	85	0.30

Table 4—Continued

RA(2000)	DEC(2000)	B	Err	V	Err	R	Err	I	Err	J ^a	Err	H ^a	Err	K ^a	Err	P	M ^b
05:38:55.425	-02:41:29.68	17.65	0.03	16.14	0.01	14.98	0.01	13.59	0.01	12.17	0.03	11.63	0.03	11.33	0.03	85	0.35
05:38:49.060	-02:38:22.51	15.05	0.01	13.99	0.01	12.96	0.01	11.41	0.03	10.68	0.03	10.50	0.03	85	0.62
05:38:25.029	-2:13:15.97	18.93	0.03	17.44	0.03	16.22	0.03	14.75	0.03	13.23	0.03	12.44	0.03	12.11	0.03	85	0.31
05:37:52.099	-02:56:55.26	20.20	0.09	18.58	0.02	17.10	0.02	15.24	0.02	13.41	0.03	12.82	0.03	12.52	0.03	85	0.18
05:39:43.188	-02:32:43.15	19.34	0.14	17.72	0.05	16.45	0.03	14.83	0.01	13.06	0.03	12.31	0.03	11.93	0.03	84	0.26
05:39:26.810	-02:19:24.66	17.12	0.02	15.64	0.02	14.60	0.02	13.44	0.02	12.16	0.03	11.38	0.03	11.13	0.03	84	0.53
05:39:02.980	-02:41:27.17	17.47	0.02	16.46	0.01	15.40	0.01	14.11	0.01	12.46	0.03	11.62	0.03	11.16	0.03	84	0.44
05:38:47.349	-02:35:25.23	14.90	0.12	13.85	0.17	12.86	0.07	84	0.68
05:38:39.550	-02:30:21.03	17.90	0.08	17.27	0.21	14.85	0.13	15.95	0.07	15.37	0.08	15.13	0.14	84	0.23
05:38:34.490	-02:41:09.10	17.76	0.07	16.18	0.15	14.72	0.04	84	0.23
05:38:28.650	-2:11:15.79	19.59	0.06	17.90	0.03	16.62	0.03	14.89	0.03	13.19	0.03	12.58	0.03	12.29	0.03	84	0.24
05:38:28.433	-03:00:26.12	19.22	0.04	17.82	0.02	16.49	0.02	14.81	0.02	13.16	0.03	12.51	0.03	12.26	0.03	84	0.24
05:38:28.433	-03:00:26.12	19.22	0.04	17.82	0.02	16.49	0.02	14.81	0.02	13.16	0.03	12.51	0.03	12.26	0.03	84	0.24
05:39:42.989	-02:13:33.18	20.17	0.06	18.58	0.02	17.25	0.02	15.56	0.02	13.94	0.03	13.30	0.03	13.01	0.03	83	0.23
05:38:49.079	-02:38:22.06	14.94	0.01	13.98	0.01	12.92	0.01	11.41	0.03	10.68	0.03	10.50	0.03	83	0.70
05:38:40.429	-02:33:27.53	17.64	0.06	16.19	0.14	14.54	0.04	12.82	0.03	12.13	0.03	11.87	0.03	83	0.22
05:38:27.639	-02:43:01.36	16.29	0.02	15.00	0.02	13.67	0.01	12.19	0.03	11.45	0.03	11.27	0.03	83	0.33
05:38:05.676	-02:40:19.36	17.96	0.04	16.43	0.02	15.34	0.01	14.07	0.01	12.80	0.03	12.24	0.03	11.96	0.03	83	0.44
05:37:45.283	-02:28:51.92	20.13	0.26	18.76	0.13	17.26	0.07	15.61	0.03	13.83	0.03	13.21	0.03	12.96	0.03	83	0.21
05:37:00.310	-02:28:26.34	19.18	0.03	17.74	0.02	16.45	0.02	14.88	0.02	13.27	0.03	12.67	0.03	12.35	0.03	83	0.27
05:36:42.656	-02:20:50.36	19.00	0.03	17.49	0.02	16.26	0.02	14.77	0.02	13.27	0.03	12.65	0.03	12.35	0.03	83	0.30
05:39:48.051	-02:45:57.02	18.10	0.04	16.58	0.02	15.49	0.01	14.18	0.01	12.94	0.03	12.27	0.03	12.04	0.03	82	0.41
05:39:32.930	-02:11:31.10	18.80	0.02	17.56	0.02	16.24	0.02	14.69	0.02	13.05	0.03	12.39	0.03	12.07	0.03	82	0.26
05:39:28.835	-02:17:51.19	18.39	0.02	16.97	0.02	15.77	0.02	14.27	0.02	12.62	0.03	11.89	0.03	11.70	0.03	82	0.30
05:39:14.491	-02:28:33.28	19.03	0.10	17.57	0.04	16.37	0.03	14.85	0.01	13.36	0.03	12.66	0.03	12.34	0.03	82	0.30
05:39:03.866	-02:20:07.85	20.09	0.06	18.79	0.02	17.38	0.02	15.62	0.02	13.84	0.03	13.17	0.03	12.89	0.03	82	0.21
05:38:45.280	-02:41:59.60	15.73	0.01	14.62	0.01	13.46	0.01	82	0.49
05:38:13.153	-02:45:50.98	16.87	0.01	15.73	0.01	14.65	0.01	13.47	0.01	12.09	0.03	11.27	0.03	10.80	0.03	82	0.49
05:37:24.292	-2:19:07.76	16.18	0.03	14.74	0.03	13.77	0.03	12.78	0.03	11.77	0.03	11.07	0.03	10.90	0.03	82	0.77
05:39:20.468	-02:27:36.72	17.43	0.03	15.93	0.01	14.81	0.01	13.52	0.01	12.16	0.03	11.43	0.03	11.17	0.03	81	0.41
05:38:49.560	-02:45:26.94	16.48	0.02	15.38	0.03	14.15	0.01	13.17	0.03	12.57	0.03	12.37	0.03	81	0.45
05:38:47.830	-02:37:19.01	15.24	0.01	14.20	0.02	13.02	0.01	11.98	0.03	11.23	0.04	10.82	0.03	81	0.52
05:38:22.959	-02:36:49.90	18.66	0.15	17.14	0.17	15.63	0.05	13.79	0.03	13.15	0.03	12.78	0.03	81	0.23
05:38:08.986	-2:20:11.24	19.15	0.04	17.66	0.03	16.41	0.03	14.85	0.03	13.25	0.03	12.60	0.03	12.31	0.03	81	0.28
05:37:49.598	-03:02:48.02	20.37	0.11	19.02	0.03	17.48	0.02	15.63	0.02	13.75	0.03	13.17	0.03	12.84	0.03	81	0.17

Table 4—Continued

RA(2000)	DEC(2000)	B	Err	V	Err	R	Err	I	Err	J ^a	Err	H ^a	Err	K ^a	Err	P	M ^b
05:39:48.578	-02:16:30.43	17.41	0.02	15.91	0.02	14.88	0.02	13.68	0.02	12.46	0.03	11.86	0.03	11.58	0.03	80	0.51
05:39:39.326	-02:32:25.15	20.35	0.34	18.78	0.13	17.34	0.07	15.52	0.02	13.47	0.03	12.91	0.03	12.56	0.03	80	0.20
05:39:08.110	-02:32:28.14	18.83	0.19	17.55	0.21	15.76	0.07	13.83	0.03	13.26	0.03	12.92	0.03	80	0.23
05:38:52.511	-2:12:21.41	19.05	0.04	17.56	0.03	16.33	0.03	14.77	0.03	80	0.28
05:38:52.241	-02:08:09.73	20.78	0.13	19.08	0.03	17.60	0.01	15.68	0.01	13.70	0.03	13.10	0.03	12.81	0.03	80	0.17
05:38:28.389	-02:30:43.04	16.05	0.05	13.90	0.07	13.43	0.01	12.80	0.03	12.40	0.03	12.31	0.03	80	0.33
05:38:25.495	-2:10:23.35	17.34	0.03	15.87	0.03	14.76	0.03	13.45	0.03	12.09	0.03	11.38	0.03	11.19	0.03	80	0.41
05:38:06.740	-02:30:22.50	16.46	0.01	15.08	0.01	14.08	0.01	13.14	0.01	11.77	0.03	10.94	0.03	10.56	0.03	80	0.79
05:38:00.960	-02:26:07.80	18.08	0.04	16.71	0.02	15.57	0.01	14.27	0.01	12.82	0.03	12.16	0.03	11.94	0.03	80	0.40
05:37:58.895	-02:26:55.96	19.76	0.18	18.65	0.11	17.49	0.09	15.64	0.03	16.01	0.07	15.35	0.07	15.07	0.14	80	0.24
05:37:56.467	-02:43:57.36	18.22	0.05	16.78	0.02	15.67	0.01	14.34	0.01	13.02	0.03	12.35	0.03	12.11	0.03	80	0.40
05:37:55.934	-02:55:17.84	18.13	0.02	16.67	0.02	15.56	0.02	14.23	0.02	12.80	0.03	12.07	0.03	11.88	0.03	80	0.40
05:39:56.023	-02:51:23.05	17.61	0.01	16.12	0.01	14.94	0.01	13.49	0.01	12.02	0.03	11.35	0.03	11.02	0.03	79	0.33
05:39:31.321	-02:48:52.76	19.72	0.16	18.18	0.07	16.86	0.05	15.20	0.02	13.63	0.03	12.94	0.03	12.67	0.03	79	0.24
05:39:14.535	-02:19:36.47	17.33	0.02	15.90	0.02	14.83	0.02	13.60	0.02	12.20	0.03	11.47	0.03	11.26	0.03	79	0.47
05:39:07.603	-02:28:23.32	18.40	0.06	16.93	0.02	15.82	0.02	14.37	0.01	12.89	0.03	12.16	0.03	11.97	0.03	79	0.35
05:39:03.589	-02:46:27.04	18.04	0.03	16.94	0.02	15.82	0.02	14.37	0.01	12.84	0.03	12.14	0.03	11.86	0.03	79	0.34
05:38:45.344	-03:04:42.89	19.95	0.05	18.43	0.01	17.11	0.01	15.43	0.01	13.84	0.03	13.26	0.03	12.90	0.03	79	0.24
05:38:20.513	-02:34:08.94	18.94	0.10	17.29	0.03	16.07	0.03	14.36	0.01	79	0.25
05:37:51.521	-02:35:25.55	15.64	0.01	14.56	0.01	13.34	0.01	11.91	0.03	11.19	0.03	10.98	0.03	79	0.47
05:39:48.913	-02:29:10.91	19.02	0.10	17.34	0.03	16.24	0.02	14.70	0.01	13.31	0.03	12.61	0.03	12.29	0.03	78	0.32
05:39:24.358	-02:34:01.25	18.19	0.05	16.62	0.02	15.53	0.01	14.28	0.01	12.96	0.03	12.27	0.03	12.05	0.03	78	0.45
05:39:11.848	-02:27:40.87	19.64	0.19	18.03	0.06	16.84	0.04	15.20	0.02	13.63	0.03	12.99	0.03	12.65	0.03	78	0.27
05:39:08.788	-02:31:11.34	19.36	0.13	17.91	0.06	16.60	0.03	14.97	0.02	13.07	0.03	12.17	0.03	11.73	0.03	78	0.25
05:38:33.280	-02:36:17.81	15.87	0.01	14.73	0.01	13.47	0.01	78	0.42
05:38:20.089	-02:38:02.17	17.49	0.06	16.02	0.06	14.33	0.02	12.60	0.03	11.87	0.03	11.63	0.03	78	0.21
05:36:50.202	-02:47:09.88	18.00	0.02	16.52	0.02	15.44	0.02	14.20	0.02	12.85	0.03	12.12	0.02	11.94	0.03	78	0.46
05:36:49.294	-02:43:54.28	19.20	0.03	17.72	0.02	16.47	0.02	14.93	0.02	13.38	0.03	12.74	0.03	12.41	0.03	78	0.28
05:36:06.042	-02:45:31.88	17.09	0.01	15.64	0.01	14.62	0.01	13.54	0.01	12.35	0.03	11.62	0.03	11.38	0.03	78	0.62
05:39:25.197	-02:38:21.98	15.88	0.01	14.72	0.01	13.78	0.01	12.83	0.01	11.31	0.03	10.46	0.03	9.98	0.03	77	0.86
05:38:32.291	-03:02:23.57	19.73	0.04	18.24	0.01	16.95	0.01	15.28	0.01	13.66	0.03	12.99	0.03	12.68	0.03	77	0.24
05:37:31.532	-02:24:26.75	17.32	0.02	15.85	0.01	14.72	0.01	13.45	0.01	12.11	0.03	11.36	0.03	11.17	0.03	77	0.41
05:39:33.792	-02:20:39.74	17.19	0.02	15.74	0.02	14.73	0.02	13.64	0.02	12.40	0.03	11.62	0.03	11.45	0.03	76	0.61
05:38:23.336	-02:44:14.14	19.87	0.25	17.99	0.06	16.92	0.05	15.19	0.02	13.46	0.03	12.84	0.03	12.57	0.03	76	0.28
05:38:00.552	-02:45:09.65	19.09	0.11	17.61	0.05	16.31	0.03	14.54	0.01	12.74	0.03	12.09	0.03	11.83	0.03	76	0.23

Table 4—Continued

RA(2000)	DEC(2000)	B	Err	V	Err	R	Err	I	Err	J ^a	Err	H ^a	Err	K ^a	Err	P	M ^b
05:37:36.667	-02:34:00.22	18.61	0.07	17.03	0.03	15.85	0.02	14.46	0.01	13.01	0.03	12.31	0.03	12.05	0.03	76	0.35
05:37:22.547	-02:59:36.50	16.47	0.01	15.06	0.01	14.13	0.01	13.15	0.01	11.80	0.02	11.09	0.03	10.83	0.03	76	0.84
05:36:29.096	-02:35:47.96	17.47	0.01	15.97	0.01	14.94	0.01	13.76	0.01	12.43	0.02	11.73	0.04	11.47	0.03	76	0.52
05:38:43.229	-02:32:00.75	17.38	0.05	15.87	0.11	14.12	0.03	75	0.20
05:38:39.812	-02:56:46.36	15.98	0.02	14.62	0.02	13.71	0.02	12.76	0.02	11.43	0.03	10.76	0.03	10.44	0.03	75	0.90
05:38:38.710	-03:07:21.52	16.90	0.01	15.42	0.01	14.45	0.01	13.41	0.01	12.28	0.03	11.58	0.03	11.35	0.03	75	0.71
05:37:44.778	-2:12:53.65	18.34	0.03	16.86	0.03	15.72	0.03	14.36	0.03	12.96	0.03	12.29	0.03	12.05	0.03	75	0.37
05:37:18.330	-02:54:09.26	19.63	0.04	18.13	0.01	16.83	0.01	15.21	0.01	13.58	0.03	12.96	0.03	12.68	0.04	75	0.25
05:38:47.790	-02:37:19.55	15.34	0.02	14.18	0.02	13.04	0.01	11.98	0.03	11.23	0.04	10.82	0.03	74	0.47
05:38:11.044	-02:56:01.76	17.28	0.02	15.83	0.02	14.73	0.02	13.46	0.02	12.09	0.03	11.30	0.03	11.13	0.03	74	0.43
05:38:11.044	-02:56:01.74	17.27	0.02	15.83	0.02	14.73	0.02	13.46	0.02	12.09	0.03	11.30	0.03	11.13	0.03	74	0.43
05:36:28.778	-02:32:58.80	20.30	0.09	18.84	0.03	17.39	0.01	15.60	0.01	13.82	0.03	13.22	0.04	12.99	0.04	74	0.20
05:39:11.541	-02:36:02.80	14.79	0.01	13.88	0.01	12.93	0.01	11.65	0.03	10.97	0.03	10.75	0.03	73	0.91
05:38:15.467	-02:03:06.62	18.08	0.01	16.57	0.01	15.51	0.01	14.28	0.01	13.07	0.03	12.38	0.03	12.15	0.03	73	0.48
05:37:42.386	-01:59:36.68	19.45	0.04	17.98	0.01	16.70	0.01	15.07	0.01	13.51	0.03	12.85	0.03	12.61	0.03	73	0.25
05:38:29.962	-2:15:40.33	19.27	0.04	17.66	0.03	16.46	0.03	14.97	0.03	13.51	0.03	12.87	0.03	12.61	0.03	72	0.31
05:37:51.874	-02:08:40.93	19.55	0.04	17.99	0.01	16.77	0.01	15.22	0.01	13.72	0.03	13.05	0.03	12.81	0.03	72	0.29
05:36:49.981	-02:35:22.62	20.05	0.05	18.45	0.02	17.12	0.02	15.49	0.02	13.94	0.03	13.29	0.03	13.05	0.04	72	0.24
05:38:36.800	-02:36:43.41	18.43	0.12	16.76	0.13	14.95	0.03	13.05	0.03	12.46	0.03	12.12	0.03	71	0.17
05:37:15.158	-02:42:01.49	19.64	0.04	18.12	0.02	16.85	0.02	15.23	0.02	13.68	0.03	13.02	0.03	12.69	0.03	71	0.26
05:36:42.557	-02:40:26.60	19.69	0.04	18.23	0.02	16.91	0.02	15.33	0.02	13.79	0.03	13.15	0.03	12.97	0.04	71	0.26
05:39:48.906	-02:29:11.02	19.02	0.10	17.33	0.03	16.23	0.02	14.71	0.01	13.31	0.03	12.61	0.03	12.29	0.03	70	0.33
05:39:37.293	-02:26:56.70	16.25	0.01	14.84	0.01	13.89	0.01	12.98	0.01	11.73	0.03	10.98	0.03	10.78	0.03	70	0.93
05:39:26.330	-02:28:37.51	19.69	0.20	18.02	0.06	16.96	0.04	15.26	0.02	13.52	0.03	12.85	0.03	12.58	0.03	70	0.29
05:39:09.282	-02:19:12.77	17.65	0.02	16.17	0.02	15.11	0.02	13.94	0.02	12.69	0.03	11.94	0.03	11.76	0.03	70	0.51
05:38:53.040	-02:38:53.53	16.29	0.01	14.86	0.01	13.85	0.01	12.78	0.01	11.62	0.03	11.03	0.03	10.80	0.03	70	0.63
05:38:50.289	-02:26:47.61	16.79	0.03	15.58	0.03	14.10	0.01	12.51	0.03	11.84	0.03	11.54	0.03	70	0.30
05:38:37.942	-02:05:52.50	16.90	0.01	15.48	0.01	14.53	0.01	13.50	0.01	12.37	0.03	11.74	0.03	11.49	0.03	70	0.75
05:38:20.130	-02:38:01.74	17.43	0.05	16.06	0.05	14.33	0.02	12.60	0.03	11.87	0.03	11.63	0.03	70	0.22
05:37:12.213	-02:03:46.54	18.34	0.02	15.56	0.01	13.55	0.01	13.19	0.01	16.16	0.11	15.72	0.16	14.82	...	70	0.43
05:38:49.789	-02:09:41.24	19.46	0.04	17.95	0.01	16.72	0.01	15.21	0.01	13.77	0.03	13.08	0.03	12.87	0.03	69	0.29
05:37:28.338	-02:24:18.50	19.31	0.04	18.11	0.02	16.75	0.02	15.34	0.02	13.98	0.03	13.38	0.03	13.06	0.04	69	0.29
05:38:44.558	-03:04:19.84	20.56	0.09	18.87	0.02	17.53	0.01	15.82	0.01	14.28	0.03	13.66	0.03	13.37	0.04	68	0.23
05:37:54.858	-02:41:09.19	19.68	0.18	18.34	0.09	17.14	0.06	15.43	0.03	13.51	0.03	12.89	0.03	12.63	0.03	68	0.25
05:39:05.247	-02:33:00.52	19.29	0.14	17.75	0.05	16.57	0.03	15.02	0.02	13.41	0.03	12.73	0.03	12.47	0.03	67	0.29

Table 4—Continued

RA(2000)	DEC(2000)	B	Err	V	Err	R	Err	I	Err	J ^a	Err	H ^a	Err	K ^a	Err	P	M ^b
05:38:33.605	-01:57:54.42	18.99	0.03	17.49	0.01	16.15	0.01	14.42	0.01	12.66	0.03	12.03	0.03	11.75	0.03	66	0.23
05:38:29.039	-02:36:02.87	16.34	0.02	15.22	0.02	14.04	0.01	63	0.47
05:38:31.595	-02:51:26.92	17.39	0.02	15.56	0.02	14.52	0.02	13.57	0.02	12.11	0.03	11.19	0.03	10.98	0.03	62	0.73
05:37:43.524	-02:09:05.17	18.59	0.02	17.02	0.01	15.86	0.01	14.47	0.01	13.11	0.03	12.48	0.03	12.24	0.03	62	0.35
05:38:01.068	-02:45:37.82	18.61	0.07	17.38	0.04	15.97	0.02	14.24	0.01	12.41	0.03	11.63	0.03	11.14	0.03	61	0.22
05:37:52.225	-02:33:37.76	18.55	0.07	16.89	0.03	15.74	0.02	14.41	0.01	12.93	0.03	12.29	0.03	12.05	0.03	61	0.38
05:38:28.314	-03:00:27.85	19.27	0.04	18.09	0.02	17.07	0.02	15.39	0.02	60	0.30
05:36:12.686	-02:40:15.32	18.88	0.03	17.31	0.01	16.04	0.01	14.46	0.01	13.06	0.03	12.44	0.04	12.18	0.03	59	0.27
05:37:37.853	-02:45:44.09	17.74	0.03	16.25	0.01	15.23	0.01	14.01	0.01	12.70	0.03	11.96	0.03	11.71	0.03	58	0.51
05:39:22.865	-02:33:32.90	17.95	0.04	16.47	0.02	15.40	0.01	14.19	0.01	12.84	0.03	12.12	0.03	11.86	0.03	57	0.48
05:38:14.878	-02:00:56.93	17.77	0.01	16.29	0.01	15.23	0.01	14.02	0.01	12.75	0.03	12.03	0.03	11.81	0.03	57	0.49
05:37:29.119	-02:40:19.87	18.48	0.05	18.15	0.08	17.04	0.05	15.44	0.03	13.86	0.03	13.24	0.03	13.06	0.04	55	0.30
05:38:28.380	-02:46:17.30	17.72	0.07	16.26	0.08	15.06	0.03	13.82	0.03	13.20	0.03	12.92	0.03	54	0.32
05:37:36.469	-2:14:37.64	16.96	0.03	15.48	0.03	14.39	0.03	13.08	0.03	11.79	0.03	11.19	0.03	10.96	0.03	54	0.41
05:37:33.158	-02:53:36.01	16.63	0.01	14.95	0.01	13.99	0.01	13.10	0.01	11.75	0.03	10.93	0.03	10.71	0.03	53	0.93
05:38:22.554	-03:11:56.78	16.73	0.01	15.89	0.01	14.94	0.01	13.83	0.01	12.34	0.03	11.41	0.03	10.87	0.03	52	0.65
05:39:47.269	-02:41:36.05	19.63	0.16	18.28	0.07	17.15	0.06	15.55	0.03	15.10	0.04	14.24	0.04	14.03	0.06	51	0.30
05:38:18.178	-01:58:42.66	20.06	0.07	18.42	0.01	17.15	0.01	15.58	0.01	14.08	0.03	13.52	0.03	13.21	0.04	51	0.27
05:38:50.094	-01:56:44.65	20.37	0.08	18.85	0.02	17.68	0.01	15.90	0.01	49	0.25
05:39:11.529	-02:31:06.46	16.31	0.01	15.32	0.01	14.40	0.01	13.45	0.01	12.02	0.03	11.21	0.03	10.74	0.03	45	0.89
05:38:58.318	-02:16:09.84	17.04	0.02	15.61	0.02	14.62	0.02	13.64	0.02	12.33	0.03	11.58	0.03	11.29	0.03	44	0.76
05:38:58.318	-02:16:09.82	17.04	0.02	15.61	0.02	14.62	0.02	13.64	0.02	12.33	0.03	11.58	0.03	11.29	0.03	44	0.76
05:38:23.351	-02:25:34.51	19.60	0.15	18.40	0.09	17.22	0.06	15.69	0.03	13.69	0.03	12.92	0.03	12.41	0.03	44	0.30
05:37:56.130	-02:09:26.54	20.64	0.10	18.92	0.02	17.49	0.01	15.68	0.01	13.90	0.03	13.29	0.03	13.04	0.03	43	0.20
05:38:49.829	-02:41:22.98	16.97	0.04	15.58	0.04	14.21	0.01	12.77	0.03	12.03	0.03	11.80	0.03	39	0.29
05:37:25.220	-2:16:04.56	19.40	0.06	17.82	0.03	16.59	0.03	15.12	0.03	13.77	0.03	13.16	0.03	12.81	0.03	39	0.30
05:39:24.013	-02:57:48.67	15.83	0.01	14.38	0.01	13.40	0.01	12.36	0.01	11.26	0.03	10.66	0.03	10.43	0.03	38	0.70
05:39:12.343	-02:30:06.34	20.44	0.44	18.17	0.08	16.69	0.04	14.69	0.01	12.64	0.03	12.06	0.03	11.74	0.03	37	0.17
05:39:05.826	-02:26:15.32	19.92	0.24	18.41	0.09	17.42	0.07	15.73	0.03	14.35	0.03	13.79	0.03	13.60	0.04	35	0.31
05:38:49.139	-02:41:24.82	15.98	0.01	14.73	0.01	13.23	0.01	11.70	0.03	11.01	0.03	10.70	0.03	34	0.29
05:39:41.738	-02:19:46.22	19.84	0.05	18.25	0.02	17.06	0.02	15.61	0.02	14.26	0.03	13.64	0.03	13.48	0.04	32	0.32
05:38:22.999	-02:36:49.48	18.33	0.11	17.24	0.13	15.67	0.05	13.79	0.03	13.15	0.03	12.78	0.03	32	0.32
05:36:21.994	-02:39:58.70	18.30	0.01	16.75	0.01	15.72	0.01	14.54	0.01	13.38	0.03	12.82	0.04	12.52	0.03	31	0.52
05:39:26.465	-02:26:15.44	18.55	0.07	17.08	0.03	15.98	0.02	14.81	0.01	13.41	0.03	12.68	0.03	12.47	0.03	30	0.49
05:39:15.054	-02:18:44.26	19.99	0.05	18.51	0.02	17.27	0.02	15.73	0.02	14.24	0.03	13.50	0.03	13.35	0.04	30	0.28

Table 4—Continued

RA(2000)	DEC(2000)	B	Err	V	Err	R	Err	I	Err	J ^a	Err	H ^a	Err	K ^a	Err	P	M ^b
05:39:17.191	-02:25:43.30	17.98	0.04	16.40	0.01	15.33	0.01	14.18	0.01	12.93	0.03	12.13	0.03	11.96	0.03	28	0.51
05:36:59.786	-02:14:52.08	17.85	0.02	16.33	0.02	15.30	0.02	14.20	0.02	12.94	0.03	12.28	0.03	12.04	0.03	28	0.57
05:39:23.944	-02:16:18.95	18.56	0.02	17.10	0.02	16.04	0.02	14.84	0.02	13.56	0.03	12.86	0.03	12.66	0.03	26	0.49
05:38:02.602	-02:04:44.41	16.45	0.01	15.06	0.01	14.16	0.01	13.24	0.01	12.04	0.03	11.38	0.03	11.16	0.03	26	0.97
05:37:23.067	-02:32:46.38	19.97	0.05	18.42	0.02	17.18	0.02	15.65	0.02	14.24	0.04	13.62	0.05	13.40	0.05	26	0.29
05:38:26.573	-2:12:17.53	16.50	0.03	15.12	0.03	14.20	0.03	13.31	0.03	11.83	0.03	10.99	0.03	10.57	0.03	24	0.98
05:38:14.482	-2:13:15.66	18.68	0.03	17.19	0.03	16.14	0.03	14.99	0.03	13.86	0.03	13.17	0.03	12.89	0.03	24	0.53
05:37:05.004	-02:41:03.43	19.86	0.04	18.30	0.02	17.10	0.02	15.68	0.02	14.33	0.03	13.78	0.04	13.50	0.05	24	0.33
05:38:53.422	-2:20:31.12	18.59	0.03	17.08	0.03	16.04	0.03	14.91	0.03	13.69	0.03	13.01	0.03	12.78	0.03	23	0.55
05:36:49.816	-02:14:38.47	16.88	0.02	15.22	0.02	14.29	0.02	13.46	0.02	12.23	0.03	11.42	0.02	11.18	0.03	21	1.06
05:37:54.004	-02:49:54.35	20.07	0.30	18.47	0.10	17.19	0.06	15.71	0.04	14.52	0.03	13.25	0.03	12.46	0.03	20	0.29
05:39:30.567	-02:38:26.96	19.36	0.13	17.82	0.05	16.61	0.03	15.21	0.02	13.82	0.03	13.18	0.03	13.00	0.03	19	0.33
05:39:42.783	-02:58:53.92	15.35	0.01	14.25	0.01	13.28	0.01	12.27	0.01	11.05	0.03	10.20	0.03	9.86	0.03	18	0.76
05:38:59.778	-02:53:57.44	17.99	0.02	16.52	0.02	15.50	0.02	14.40	0.02	13.18	0.03	12.50	0.03	12.32	0.03	18	0.58
05:38:32.758	-02:04:50.71	17.96	0.01	16.54	0.01	15.52	0.01	14.33	0.01	13.13	0.03	12.52	0.03	12.30	0.03	17	0.52
05:38:18.170	-02:43:34.85	18.63	0.13	17.52	0.08	16.00	0.05	14.68	0.03	14.08	0.03	13.81	0.05	16	0.32
05:38:59.216	-02:33:51.44	18.24	0.04	17.14	0.03	16.09	0.02	14.83	0.01	12.90	0.03	11.99	0.03	11.40	0.03	15	0.47
05:38:14.552	-2:10:15.43	18.22	0.03	16.75	0.03	15.50	0.03	13.98	0.03	12.49	0.03	11.80	0.03	11.54	0.03	15	0.29
05:36:50.626	-02:18:58.39	18.74	0.02	17.23	0.02	16.18	0.02	15.07	0.02	13.92	0.03	13.31	0.03	13.01	0.04	14	0.56
05:38:42.750	-02:38:52.84	17.21	0.05	16.03	0.10	14.92	0.04	12	0.47
05:38:41.405	-2:17:01.96	18.66	0.03	17.16	0.03	16.08	0.03	14.73	0.03	13.52	0.03	12.91	0.03	12.60	0.04	12	0.41
05:38:19.347	-02:32:04.13	19.71	0.16	18.85	0.15	17.28	0.07	15.99	0.04	14.66	0.04	14.06	0.04	13.73	0.06	12	0.27
05:38:13.194	-02:26:08.77	18.41	0.05	16.92	0.03	15.67	0.02	14.10	0.01	12.50	0.03	11.82	0.03	11.57	0.03	12	0.28
05:35:49.990	-02:35:45.32	19.40	0.04	18.19	0.01	17.01	0.01	15.58	0.01	14.18	0.04	13.61	0.03	13.32	0.04	12	0.33

^aFrom 2MASS which is available at <http://www.ipac.caltech.edu/2mass>.^bMasses were estimated from the observed $V-I_C$ using a 2.5 Myr isochrone.

Table 5. Likely Members of the σ Ori Cluster with $M \geq 3 M_{\odot}$

Name	RA	DEC	Sp. Type	$M(M_{\odot})^{\dagger}$	D(')
σ Ori A	05 38 44.768	-02 36 00.08	O9.5V	20	0
σ Ori B	05 38 44.768	-02 36 00.08	B0.5V	15	0
σ Ori D	05 38 45.510	-02 35 58.70	B2V	8	0.2
σ Ori E	05 38 47.194	-02 35 40.54	B2V	8	0.7
HD294271	05 38 36.549	-02 33 12.74	B5V	6	3.5
HD294272	05 38 34.411	-02 34 15.88	B8V	4	3.1
HD37525	05 39 01.501	-02 38 56.45	B5V	6	5.1
HD37633	05 39 46.188	-02 40 32.20	B9V	3.5	16.0
HD37333	05 37 40.481	-02 26 37.16	A0V	3	18.6
HD37545	05 39 09.216	-02 56 35.01	B9V	3.5	21.5
HD37686	05 40 13.073	-02 30 53.29	B9V	3.5	22.7
HD37699	05 40 20.210	-02 26 07.12	B5V	6	25.8
HD37744	05 40 37.325	-02 49 30.48	B1.5V	10	31.2

[†]Masses estimated from the spectral types given by Brown, de Geus, & de Zeeuw (1994)

Note. — The first four columns are from Brown, de Geus, & de Zeeuw (1994).